OUKA
The University of Osaka
Institutional Knowledge Archive

Title	Sphingomyelin metabolism underlies Ras excitability for efficient cell migration and chemotaxis
Author(s)	Shin, Da Young
Citation	大阪大学, 2023, 博士論文
Version Type	VoR
URL	https://doi.org/10.18910/93026
rights	
Note	

The University of Osaka Institutional Knowledge Archive : OUKA

https://ir.library.osaka-u.ac.jp/

The University of Osaka

Sphingomyelin metabolism underlies Ras excitability for efficient cell migration and chemotaxis

Department of Biological Science, Graduate School of Science,
Osaka University

Da young SHIN

Contents

Abstract … 1

Abbreviations … 2

1 Introduction … 3

- 1.1 *Dictyostelium discoideum*, chemotaxis and spontaneous migration
- 1.2 Excitable signaling network
- 1.3 Ras/phosphatidylinositol lipids signaling network and Sphingomyelin, Phosphatidylserine of the cell membrane
- 1.4 Results summary

2 Materials and Methods … 11

3 Results … 16

- 3.1 Self-organization of the anterior-posterior polarity required sphingomyelin metabolism
- 3.2 The excitability of Ras was suppressed by fendiline
- 3.3 The activation of Ras was suppressed by fendiline
- 3.4 Traveling waves were not recovered by an over-expression of Ras
- 3.5 Traveling waves were recovered by eliminating accumulated SM or supplementation with PS
- 3.6 Cell motility required sphingomyelin metabolism
- 3.7 Conditions of fixation
- 3.8 The number densities of Ras-GTP molecules and clusters were reduced by fendiline

4 Discussion … 47

References … 49

Publication List … 54

Acknowledgements… 55

Abstract

In eukaryotic motile cells, the active Ras (Ras-GTP)-enriched domain is generated in an asymmetric manner on the cell membrane through the excitable dynamics of an intracellular signaling network. This asymmetric Ras signaling regulates pseudopod formation for both spontaneous random migration and chemoattractant-induced directional migration. While membrane lipids, such as sphingomyelin and phosphatidylserine, contribute to Ras signaling in various cell types, whether they are involved in the Ras excitability for cell motility is unknown. Here I report that functional Ras excitability requires the normal metabolism of sphingomyelin for efficient cell motility and chemotaxis. The pharmacological blockade of sphingomyelin metabolism by an acid-sphingomyelinase inhibitor, fendiline, and other inhibitors suppressed the excitable generation of the stable Ras-GTP-enriched domain. The suppressed excitability failed to invoke enough basal motility to achieve directed migration under shallow chemoattractant gradients. The fendiline-induced defects in Ras excitability, motility and stimulation-elicited directionality were due to an accumulation of sphingomyelin on the membrane, which could be recovered by exogenous sphingomyelinase or phosphatidylserine without changing the expression of Ras. These results indicate a novel regulatory mechanism of the excitable system by membrane lipids, in which sphingomyelin metabolism provides a membrane environment to ensure Ras excitation for efficient cellular motility and chemotaxis.

Abbreviations

cAMP	Cyclic adenosine monophosphate
DB	Development Buffer
DB(-)	Development Buffer without $CaCl_2$ and $MgCl_2$
GFP	Green fluorescent protein
HL5	HL5, the medium for Dictyostelium Discoideum
LatA	Latrunculin A
PALM	Photo-activated localization microscopy
TIRFM	Total internal reflection fluorescence microscope
PHD	PH domain, Pleckstrin homology domain
PI3K	Phosphoinositide 3-kinase
PIP2	Phosphatidylinositol (4,5)-biphosphate
PIP3	Phosphatidylinositol (3,4,5)-triphosphate
PTEN	Phosphatase and tensin homolog
PS	Phosphatidylserine
SM	Sphingomyelin metabolism
TMR	Tetramethylrhodamine

Introduction

1.1 *Dictyostelium discoideum*, chemotaxis and spontaneous migration

Slime molds are a group of unicellular, spore-producing eukaryotic organisms. Slime molds live in moist, rotting organic matter, and can be found by examining dead trees or piles of fallen leaves. It looks very primitive, but it is a eukaryote and has a unique and diverse life history. The life cycle of this fungus is a free-swimming amoeba that grows and proliferates, and when external nutrients are exhausted, amoebas are attracted to chemicals released by fellow amoebas to form multicellular colonies. After that, the stalk and spore are formed through the developmental stage, and the stalk is senescent, the spore exists in a dormant state. Afterwards, the spore wall is destroyed and amoebas appear [1].

One of the model organisms for collective cell migration is social amoebae, *Dictyostelium discoideum*. There are many kinds of collective motion in nature, but one of the most studied collective motions in biology is cooperative behavior of multiple cells, namely collective cell migration (Fig.1). When *D. discoideum* cells become a nutrient starvation environment and forms a multicellular body from unicellular phase, it moves towards a high concentration in response to the gradient of chemical substances in the external environment [2][3]. In this case, the chemical is cAMP, and such movement is called chemotaxis [4][5]. In addition, these cells can move in their own direction without being instructed from the outside, and this is called spontaneous movement. On the front side of the cell, a structure called pseudopodia is created to push the membrane forward. On the posterior side, the membrane is shortened [6][7][8][9]. Cells are made up of molecules such as proteins, lipids, and carbohydrates, so the molecules should determine the anterior and posterior of the cell.

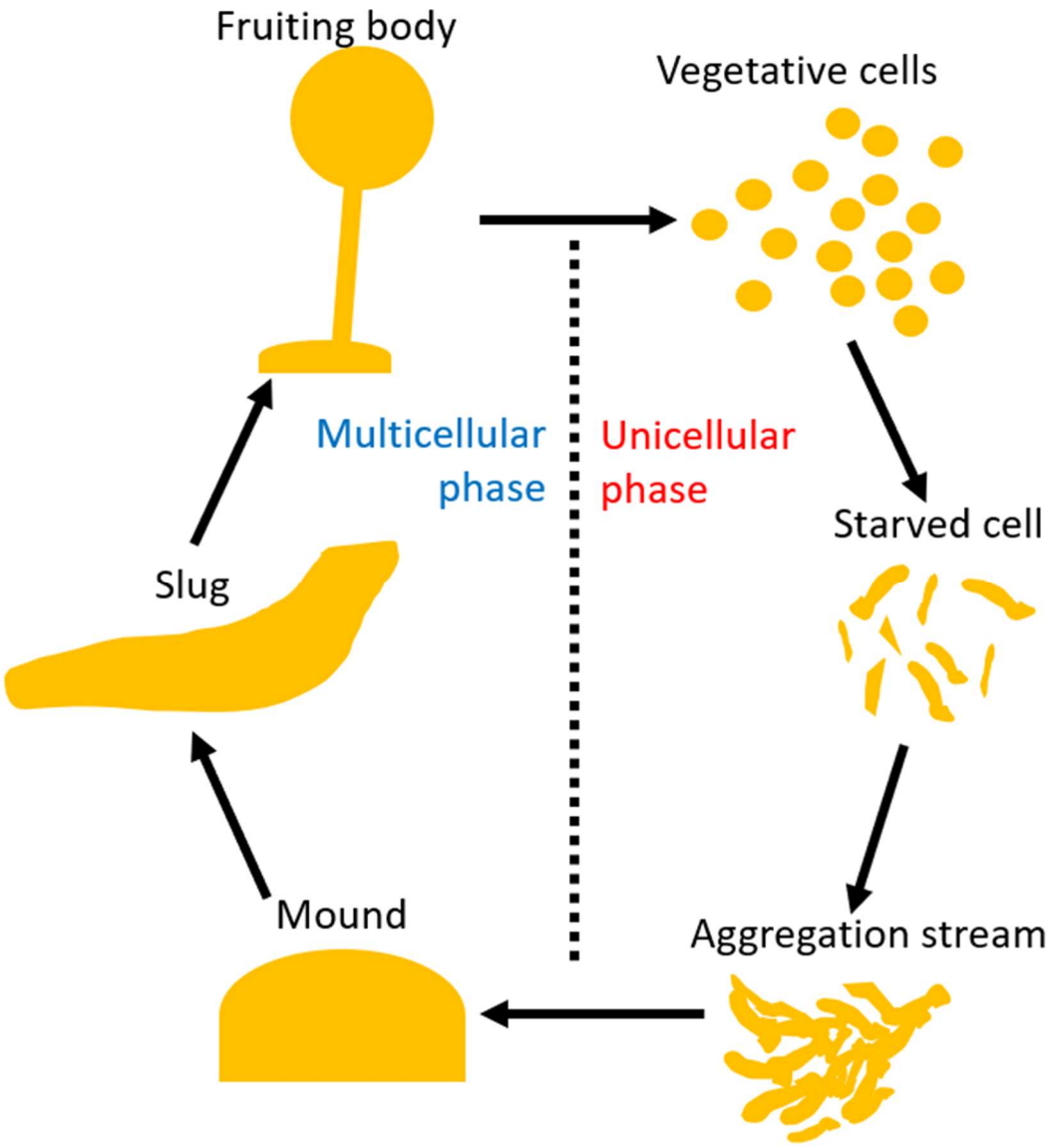


Figure 1. Life cycle of *Dictyostelium discoideum*.

1.2 Excitable signaling network

An anterior-posterior polarity formation in eukaryotic motile cells is one example of the self-organization essential in living systems [10][11][12][13]. The cells migrate spontaneously in spatially uniform environment. A domain in which specific signaling molecules are enriched is self-organized on the cell membrane, activating anterior signaling events that lead to pseudopodia formation [14][15][16]. These signaling molecules include a small GTPase, Ras, in an active form (Ras-GTP), PI 3-kinase, phosphatidylinositol 3,4,5-trisphosphate (PIP3) and Pleckstrin homology (PH)-domain-containing proteins that bind to PIP3 such as PKB/Akt. Previous studies using *D. discoideum* as a model organism have revealed that neither extracellular spatial signals nor cellular cytoskeletal polarity are prerequisite for the domain formation, which is observed in the immobilized cells with an actin polymerization inhibitor [10][17]. The same self-organization mechanism underlies chemotaxis in response to extracellular concentration gradient of chemoattractant, which generates the domain at the cell side facing to the higher concentration and thus determines the moving direction [18][19]. The self-organization of the domain is based on an excitable system [20], which is responsible for spontaneous signal generation with a stereotypical spatiotemporal pattern from stochastic noises [21][22]. So far, the molecular mechanism of the excitable system has not been elucidated and awaited a quantitative analysis of the noise.

An excitable system exhibits different spatiotemporal dynamics depending on the conditions (Fig.2) [19]. The excitatory dynamics is observed under the sub-threshold conditions. The system adopts a stable resting state with a low level of the output signal unless stochastic fluctuations of the signal cross a threshold. When crosses the threshold, the signal level exhibits a transient excursion from the original resting-state level with a stereotypical spatiotemporal pattern. Thus, the intrinsic noise causes the excitation, which is a reason why the pattern emerges spontaneously and stochastically. *D. discoideum* cells under the physiological conditions are thought to utilize the excitable dynamics for the generation of the domain in spontaneous cell migration without any extrinsic stimulus [19]. The domain appeared on the membrane is stabilized at the front for a while due to a positive feedback loop through activating actin polymerization and accepting feedback from the actin cytoskeleton, and thus any oscillatory properties are hardly observed under the conditions. On the other hand, the oscillatory dynamics is observed under the supra-threshold conditions. The conditions with enough small distance between the resting-state signal level and the threshold or

enough large magnitude of the noise ensure repetitive excitations one after another, leading to spatiotemporal oscillations such as traveling waves. The transition from the excitatory into oscillatory dynamics can be induced via modulations to enhance the excitability of the system by raising the resting-state signal level, lowering the threshold, or increasing the noise magnitude. Empirically, *D. discoideum* cells are treated with caffeine to enhance the excitability [10][17]. Traveling waves of Ras-GTP, PI 3-kinase, PTEN, PIP3 and phosphatidylinositol 4,5-bisphosphate (PIP2) emerge robustly in its presence, which enabled quantitative imaging analysis, and a molecular network model with Ras at its core was revealed [23]. Thus, the noise associated with the Ras signaling has gained attention as being critical for the excitability. However, there have been little studies considering the link between the exact origin of the molecular noise and the excitability in the living cells.

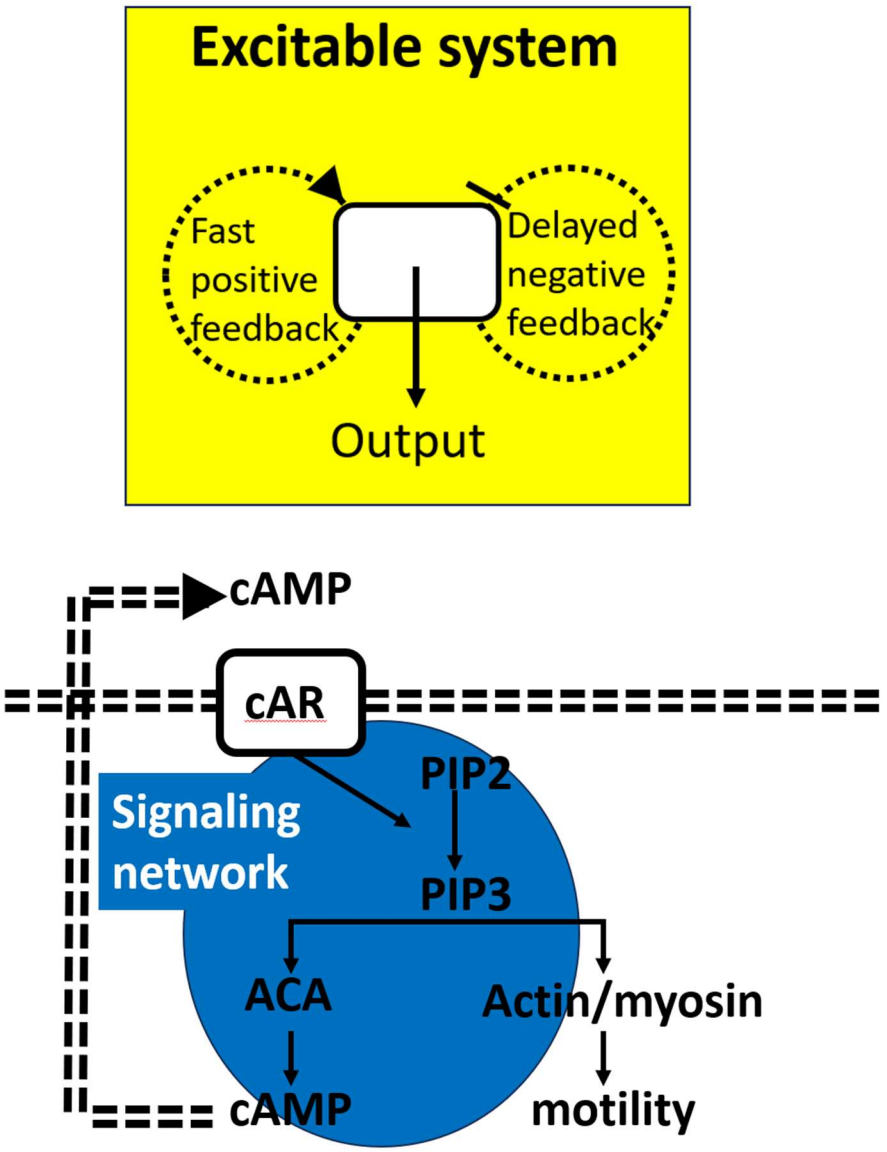


Figure 2. Diagram of signaling circuit for excitable system and signaling system of cell motility.

1.3 Ras/phosphatidylinositol lipids signaling network and Sphingomyelin, Phosphatidylserine of the cell membrane

The major sources of the molecular noise associated with the Ras signaling potentially include the reactions of the membrane association and dissociation and the activation and inactivation via GDP/GTP exchange as well as lateral diffusion on the cell membrane. Intensive studies on mammalian K-Ras, with which the Ras proteins in *D. discoideum*, RasG and RasC, share similar structures, have revealed that the C-terminal anchor sequence composed of a polybasic stretch and a prenylated CAAX motif is critical for the localization and spatial distribution on the cell membrane, where phosphatidylserine (PS) plays an essential role [26][27]. The PS level on an inner leaflet of the cell membrane is regulated dependently on a precise metabolism of sphingomyelin (SM) [28][29]. The metabolic reactions involving SM comprise a cycle coupled with intracellular vesicle trafficking [30]. SM is produced from ceramide (Cer) by SM synthase (SMS) on the Golgi membrane and transported to the cell membrane. SM is degraded to Cer by neutral sphingomyelinase (nSMase) on the cell membrane and acid sphingomyelinase (aSMase) on the endosome and lysosome membranes. Cer is degraded to sphingosine, which is further used to produce sphingosine-1-phosphate by sphingosine kinase on the cell membrane. Sphingosine on the lysosome membrane enters a salvage pathway and is used to produce Cer by Cer synthase (CerS) on the endoplasmic reticulum, where Cer is also synthesized de novo from serine and palmitoyl-CoA by serine palmitoyl transferase (SPT), CerS and other enzymes. Cer is transported to the Golgi. Some chemical compounds cause an accumulation of SM on the endomembrane in mammalian cultured cells such as fendiline, desipramine, amitriptyline and imipramine, inhibitors of aSMase, and D609 and 2-OHOA, an inhibitor and an activator of SMS, respectively [28][29][31]. Other compounds such as SKI-II and L-threo-DHS, inhibitors of sphingosine kinase I and I/II, respectively, increase the SM level on the cell membrane. The other compounds such as fumonisin B1, an inhibitor of CerS, and myriocin, an inhibitor of SPT, reduce the cellular SM content. Irrespective of these varying effects upon SM levels and distribution, all these compounds reduce the PS level and suppress the localization of K-Ras-G12V on cell membrane [29]. In addition, K-Ras is known to form clusters depending on the interaction between the C-terminal anchor and PS, but these compounds cause de-clustering of K-Ras consistently due to the reduction of PS [26][27][29][32][33][34][35]. It has been proposed that the physiological role of clustering is to establish low-noise and high-fidelity signal transmission in the confined region for the case of K-Ras signaling [36][37]. On the other hand, it is unclear whether the excitable system of Ras in the

cellular polarity formation requires similar clustered structures. Especially, the Ras-GTP-enriched domain generated upon the excitation spans around 10 μm, while the size of the K-Ras cluster is reported to be less than 50 nm, suggesting a large gap in the characteristic size [29][32][35]. To elucidate the molecular mechanism of the excitation, it is required to quantitatively analyze the causal relationship between the magnitude of the molecular noise arises in the spatial distribution and the excitable dynamics.

1.4 Result summary

This study has revealed that an accurate SM metabolism offers an optimal membrane environment for Ras activation in the excitable system of motile cells. The same chemicals as those reported to suppress K-Ras signaling were shown to suppress the Ras signaling for spontaneous cellular polarity formation in *D. discoideum*. Fendiline, exploited as the representative, suppressed the excitability, and the reduction of the number density of Ras-GTP on the membrane was quantitatively confirmed in the fendiline treated cells by photo-activated localization microscopy (PALM). PALM also revealed the clusters of Ras-GTP with a mean radius of approximately 200 nm. The results demonstrate that SM metabolism contributes to the augmentation of molecular noise so that spontaneous signal generation is ensured for intrinsic cell motility and chemotactic responses. This study proposes a novel mechanism of excitability-based self-organization in living systems involving dynamic mesoscopic structures.

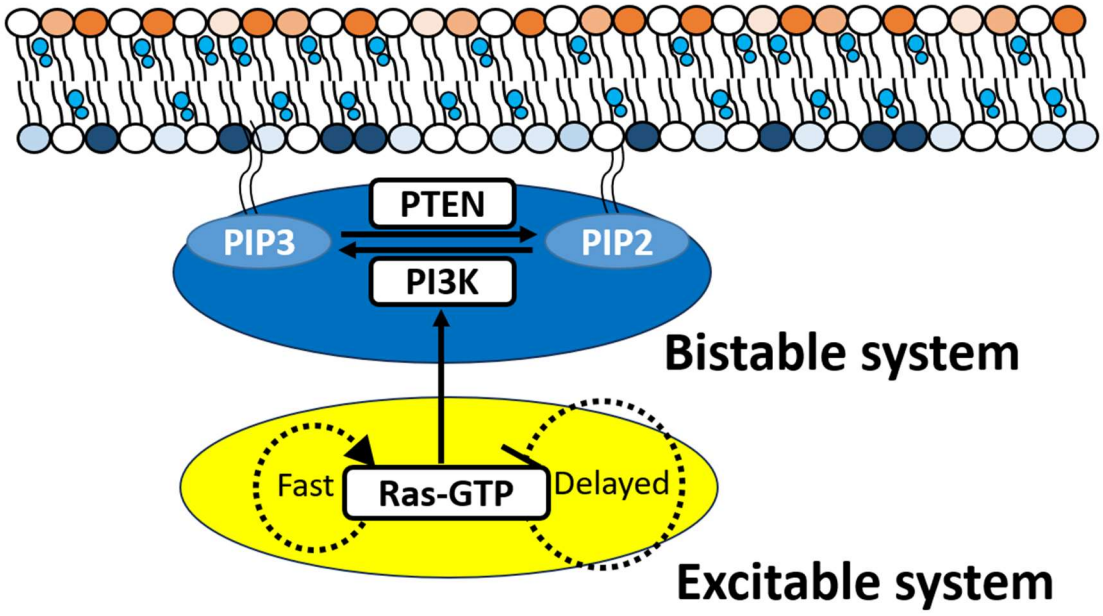


Figure 3. Scheme of the signaling network investigated in this study.

Materials and Methods

Cell strains and culture

Dictyostelium discoideum wild-type strain Ax2 (dictyBase strain ID: DBS0235518) was used as the parental cell line throughout this study. The cells were cultured in HL5 medium (15.4 g glucose, 7.15 g yeast extract, 14.3 g proteose peptone No.2, 0.485 g KH_2PO_4, 1.28 g $Na_2HPO_412H_2O$, 0.2 mg folic acid, and 0.06 mg cyanocobalamin per L) supplemented with penicillin and streptomycin at 21 °C. The cells in which the plasmids were introduced were selected and maintained in the presence of G-418 (20 mg/mL; Wako), Blasticidin S (10 mg/mL; Invivogen) or Hygromycin B (50 mg/mL; Wako). The cell strain overexpressing RasG and RBD_{Raf1}-GFP simultaneously was maintained in the presence of 14 mg/mL G-418 and 35 mg/mL Hygromycin B to allow cell growth. The plasmids for the overexpression of RBD_{Raf1}-GFP and the simultaneous overexpression of $PHD_{PKB/Akt}$-GFP and PTEN-Halo are described elsewhere [23][37]. Inhibitors and activators of SM metabolism were kept as stock solutions dissolved in DMSO at -30 °C and added to HL5 at the indicated final concentrations, which included fendiline hydrochloride (Santa Cruz), desipramine hydrochloride (TOCRIS), amitriptyline hydrochloride (TOCRIS), imipramine hydrochloride (Nacalai), L-DHS (Sigma), SKI-II (Echelon), D609 (Cayman), 2-OHOA (Sigma), fumonisin B1 (Cayman), and myriocin (Cayman).

Cell preparation

Starved cells were used throughout the study and prepared as follows. Cultured cells were washed twice with development buffer (DB; 5 mM Na/KPO_4, 2 mM $MgSO_4$, and 0.2 mM $CaCl_2$, pH 6.5) by centrifugation (500xg, 2 min) and suspended in DB at a cell density of $3x10^6$ cells/mL. 1 mL of cell suspension was transferred to a 35 mm culture dish and kept still for 3 hours at 21 °C. For the treatment with SMase during the starvation period, 1 μL SMase from Staphylococcus aureus (S8633; Sigma-Aldrich) was added to the 35-mm culture dish. To observe PTEN-Halo, HaloTag® TMR ligand (Promega) was added to the cell suspension at final concentrations of 2 μM during the last 30 min. The starved cells were washed twice with DB by centrifugation, suspended in DB at around $5x10^6$ cells/mL and kept on ice until used. The cells were cultured in a 96-well glass bottom dish (Greiner) in the presence of the inhibitors and starved in the well by replacing HL5 medium with DB.

Lysenin staining

100 μL cell suspension in DB containing 10 μM latrunculin A with/without fendiline and SMase was put on a coverslip and incubated for 30 min in a moist chamber. The coverslip was soaked in DB containing 4% paraformaldehyde, 0.2% glutaraldehyde and 0.1% Triton-X prechilled on ice for 5 min. The cells were further fixed with the same fixatives dissolved in DB without calcium and magnesium ions (DB(-)) for 5 min on ice. The coverslip was washed with DB(-) three times. After an excess fluid was removed, the cells were covered with 100 L DB(-) containing mCherry-Lysenin and incubated for 10 min in a moist chamber. The fluid was removed, and the coverslip was washed with DB and observed by confocal microscopy. mCherry-Lysenin was prepared according to the provider's protocol [43].

Western blotting

The starved cells were suspended in DB and lysed by passing through a doubled filter membranes (Whatman Nucleopore Track-etched membrane, Merck). The lysate was mixed with sample buffer, boiled for 5 min and stored at −30 °C. The sample derived from $7.5x10^4$ cells was subjected to SDS-PAGE in a precast gel (SuperSep Ace 5–20%, Wako) and blotted onto a PVDF membrane (Immobilon-P, Millipore). The membrane was treated with 5% (w/v) skim milk/TBS-T (Tris-buffered saline containing 0.05% Tween-20) for 1 h at room temperature (RT), washed with TBS-T, and reacted with anti-Pan-Ras mouse monoclonal antibody (OP40; Calbiochem) diluted with TBS-T at 1:2000 for 1 h at RT. The membrane was washed with TBS-T and reacted with horseradish peroxidase (HRP)-conjugated anti-mouse IgG (NA931, GE Healthcare) diluted with TBS-T at 1:5000 for 1 h at RT. After washing with TBS-T, signals were detected by using ECL Prime (GE Healthcare).

Confocal laser scanning microscopy

Cell suspension containing 10 μM latrunculin A (Sigma) and 4 mM caffeine (Wako) was placed on a coverslip of a 35-mm glass bottom dish (12-mm glass in diameter, Iwaki). The cells were allowed to settle by a 30-min incubation and then observed under laser confocal microscopy (A1, Nikon). For the removal of fendiline before microscopic observation of RBD_{Raf1}-GFP, starved cells in 200 μL suspension containing fendiline was placed on the coverslip, incubated for 30 min, washed 3 times with DB and incubated in DB without fendiline for 30 min. For the treatment with SMase or PS before microscopic observation of RBD_{Raf1}-GFP, 200 μL cell suspension was placed on the coverslip, incubated for 30 min and mixed with 100 μL DB containing 0.45 μL

SMase or 3 uL PS solution. PS solution was prepared as follows: 15 μL Brain PS (10 mg/mL dissolved in chloroform, 840032C, Avanti Polar Lipids) was dried under a vacuum in a glass vial to remove the solvent and redissolved in 60 μL Dulbecco's phosphate buffered saline (14190144, Gibco, ThermoFisher Scientific) containing 0.01% BSA (017-15146, Fujifilm) by sonication for 30 min. PS solution diluted with DB was centrifuged at 10,000-xg for 1 min, which supernatant was added to the cells. The movies were acquired at 5-s intervals for 30 min.

Spatiotemporal dynamics analysis

The fluorescence intensities of RBD_{Raf1}-GFP, $PHD_{PKB/Akt}$-GFP and TMR conjugated to PTEN-Halo in an arbitrary ROI in the confocal images were measured using Fiji.

Cell motility imaging

A 600 μL cell suspension was placed on a coverslip set in an Attofluor^{TM} cell chamber. The cells were allowed to adhere to the surface by a 20 min incubation. DB was replaced with new DB to discard unattached cells. After another incubation for 10 min, the cells were observed under an inverted microscope (IX71, Olympus) equipped with a time-lapse camera (DS-2MBW, Nikon). For the removal of fendiline, starved cells in 600 μL suspension containing fendiline was placed on the coverslip, incubated for 30 min, washed 3 times with DB and incubated in 600 μL DB without fendiline for 30 min. For the treatment with SMase or PS, 600 μL cell suspension was placed on the coverslip, incubated for 30 min, replaced with 600 μL DB containing 0.9 μL SMase or 6 μL PS solution and incubated for 30 min. A concentration gradient of cAMP was applied with a glass micropipette using FemtoJet (Femtotips II, Eppendorf). DB containing 100 nM cAMP filled in the glass micropipette was released by applying pressure at 50 hPa. The images were acquired at 5-s intervals for 30 min.

Cell motility analysis

The *x*- and *y*-coordinates of a cell were determined automatically using a Fiji plugin, TrackMate, to generate a migration trajectory [36]. The net displacement over 30 min was used to calculate the migration speed of the cell.

Photo-activated localization microscopy

Prior to the experiments, the coverslips were coated with gold colloids for the purpose of calibration of the stage position, which often shows a drift during PALM image acquisition. The coverslips were cleaned by sonication in 0.1 N KOH for 60 min,

washed with distilled water three times, and sonicated in distilled water for 5 min three times. The coverslips were soaked in EtOH (99.5%), which was replaced with fresh EtOH twice. The coverslips were treated with 3%(v/v) (3-Aminopropyl)triethoxysilane (Sigma-Aldrich) dissolved in EtOH for 45 min at room temperature by gentle shaking. The coverslips were washed with distilled water three times, and excess water was removed. 20 μL gold colloid solution (100 nm, BBI; diluted 4-fold with distilled water) was sandwiched between the two coverslips and incubated for 2 h in a moist chamber. After washing with distilled water three times, the coverslips were treated with 4% sodium silicate solution (Sigma-Aldrich; pH was adjusted to 8.5 with Amberlite IR-120) for 2 h at 95°C. The coverslips were washed with distilled water three times, and the adsorption of the gold colloids was checked by TIRFM.

A 10 mL cell suspension was placed on the coverslip, and the cells were allowed to adhere to the surface by incubating the coverslip in a moist chamber for 10 min. The cells were overlaid with a 1 cm^2 agarose sheet made of 2% low melt agarose (Amersham Pharmacia Biotech) dissolved in DB without Ca^{2+} or Mg^{2+}. Excess fluid was removed with filter paper. After incubation in a moist chamber for 30 min, the coverslip was dipped in HL5 buffer (0.485 g KH_2PO_4, and 1.28 g $Na_2HPO_412H_2O$ per L) containing 4% paraformaldehyde, 0.25 % glutaraldehyde, and 0.1% Triton X-100 for 10 min at room temperature. The coverslip was washed with DB three times and soaked in 1 mg/mL $NaBH_4$ for 3 min. After washing with DB three times, the coverslip was air-dried overnight. The dried coverslip was set in an Attofluor™ cell chamber (ThermoFisher Scientific), filled with DB and observed by PALM. The detailed configuration of the microscope system is described elsewhere [37]. Briefly, objective type TIRFM was constructed on an inverted fluorescence microscope (T*i*, Nikon) equipped with an EMCCD camera (iXon3, Andor), a 405 nm laser for a photoactivation (Cube 405-50C, Coherent), a 488 nm laser for excitation before photoactivation (Sapphire 488-50, Coherent), and a 561 nm laser for excitation after photoactivation (Sapphire 561-150 LS, Coherent). The images were acquired until all the fluorophores were photobleached. The intensity of the 405 nm laser was automatically increased with time using laboratory-made software.

Ripley's L function:

Let n be the number of molecules in a cell and I ($d_{ij} < r$) be the number of molecules within distance r from each molecule, then Ripley's K function is defined by the following equation:

$$\mathrm{K}(r) = \frac{\pi r^2}{n} \sum_{i=1}^{n} \sum_{i \neq j}^{n} \frac{I(d_{ij} < r)}{n-1}$$

Based on Ripley's K function, Ripley's L function is defined as

$$L(r) = \sqrt{\frac{K(r)}{\pi}} - r$$

If the spatial distribution of the molecules is uniformly random, then $L(r) = 0$. If there is a spatial scale where the molecules are more dense than uniformly random, then $L(r) > 0$ at that scale.

Hierarchical clustering:

Based on the position of the molecules, hierarchical clustering was performed using the group average method to create a histogram of the size and number of clusters on a 200 nm scale. For hierarchical clustering, the hclust function in R was used.

Hopkins-Skellam index:

Let n be the number of molecules in a cell, r_{1i} be the shortest distance between molecule i and other molecules, and r_{2i} be the shortest distance between an artificial point randomly placed in the cell region and n real molecules. Then, HSI (Hopkins-Skellam Index) is defined by the following equation based on the sum of n points:

$$HSI = \frac{\sum_{i=1}^{n} r_{2i}^2}{\sum_{i=1}^{n} r_{1i}^2}$$

If HSI=1, the molecules show a uniformly random distribution in space; if HSI<1, the molecules are more dispersed than uniformly random; and if HSI>1, the molecules are more localized than uniformly random.

Results

3.1 Self-organization of the anterior-posterior polarity required sphingomyelin metabolism

I investigated an involvement of SM metabolism in the generation of anterior-posterior polarity in *D. discoideum* cells. The distributions of PIP3 and PTEN, anterior and posterior signaling molecules, respectively, were examined in cells expressing the GFP-tagged PH domain of PKB/Akt ($PHD_{PKB/Akt}$-GFP) and tetramethylrhodamine (TMR)-labeled HaloTag®-tagged PTEN (PTEN-Halo) after cultivation in the presence of SM metabolism inhibitors or activators [37][38][39]. The cells were treated with 5 mM latrunculin A and 4 mM caffeine to reduce the cellular morphological anisotropy and suppress autonomous chemoattractant signaling, respectively, and observed under confocal laser scanning microscopy [10]. The spontaneous generation of PIP3/PTEN polarity was observed in most (71%) cells cultured in control medium containing dimethyl sulfoxide (DMSO), in which PIP3-enriched and PTEN-enriched domains existed in a mutually exclusive manner on the cell membrane (Fig. 4A). When the cells were cultured in the presence of the drugs, the fraction of cells showing PIP3/PTEN polarity was reduced in a dose-dependent and cultivation time-dependent manner (Fig. 5). In these cells, the membrane localization of $PHD_{PKB/Akt}$ but not of PTEN was suppressed (Fig. 4B, 4C), indicating that the drugs suppressed the signaling pathway of PI3K but not of PTEN.

An active form of RasG, which is an upstream regulator of PI3K in *D. discoideum*, can be detected by the Ras-binding domain of Raf1 (RBD_{Raf1}) tagged with GFP (RBD_{Raf1}-GFP) [40]. The spontaneous generation of Ras-GTP polarity was observed in 75% of RBD_{Raf1}-GFP-expressing cells cultured in control medium, in which a Ras-GTP-enriched domain was formed on the cell membrane (Fig. 4D, 4E). The fraction of cells showing this polarity was reduced to 18~38% after treatment with SM metabolism inhibitors. Therefore, the spontaneous generation of Ras-GTP polarity and thus PIP3/PTEN polarity requires SM metabolism.

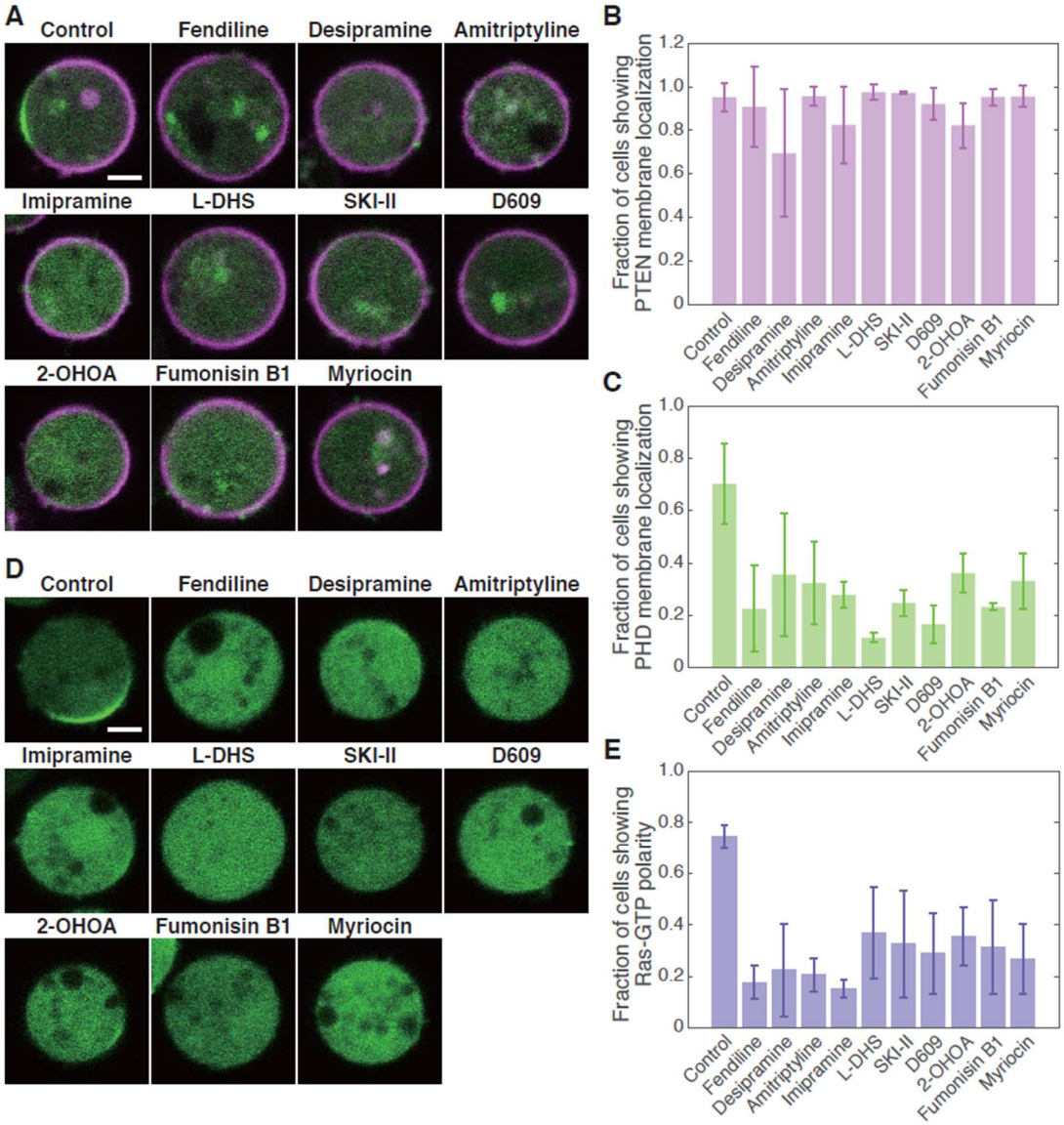


Figure 4. Self-organization of PIP3/PTEN and Ras-GTP polarity was suppressed by the pharmacological blockade of SM metabolism.

(A) Representative images of cells expressing $PHD_{PKB/Akt}$-GFP and PTEN-Halo after drug treatment. (B) Fraction of cells showing PTEN membrane localization. P = 0.678, 0.428, 0.903, 0.339, 0.606, 0.609, 0.671, 0.087, 0.969 and 0.949 (control versus fendiline, desipramine, amitriptyline, imipramine, L-DHS, SKI-II, D609, 2-OHOA, fumonisin B1 and myriocin, respectively) by Welch's t test. (C) Fraction of cells showing $PHD_{PKB/Akt}$ membrane localization. P = 0.006, 0.245, 0.009, 0.008, 0.004, 0.006, 0.005, 0.014, 0.008 and 0.013. (D) Representative images of cells expressing RBD_{Raf1}-GFP after drug treatment. (E) Fraction of cells showing Ras-GTP polarity. P =

0.000, 0.008, 0.001, 0.000, 0.059, 0.066, 0.028, 0.015, 0.047 and 0.017. The cells were cultured in the presence of the indicated drug for 48 hours at 10^{-5} M and treated with 5 μM latrunculin A and 4 mM caffeine. Scale bars, 3 μm. Error bars, SD.

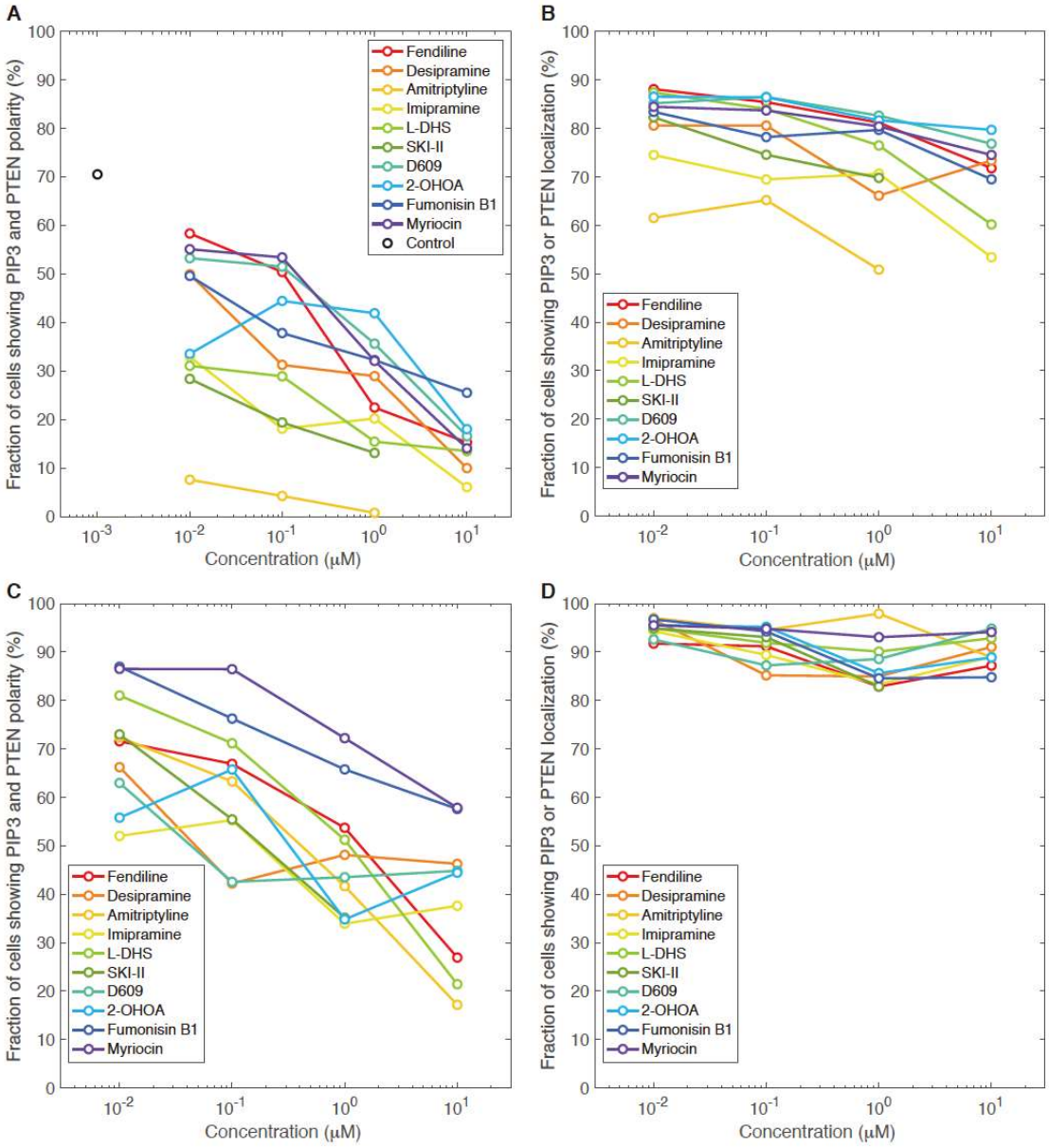


Figure 5. Dose-dependent effects of inhibitors and activators of SM metabolism on the spontaneous generation of cellular polarity.

The cells were cultured in the presence of the SM metabolism inhibitors and activators at the indicated concentrations for 48 hours (A, B) or 24 hours (C, D). The fraction of cells showing both PHD and PTEN membrane localization (A, C) and the membrane localization of either PHD or PTEN (B, D) are shown.

3.2 The excitability of Ras was suppressed by fendiline

To investigate the involvement of SM metabolism in the cellular polarity formation in detail, fendiline, an inhibitor of acid sphingomyelinase (SMase), was used as a representative hereafter [31]. Because the spontaneous generation of cellular polarity is underpinned by the excitability of Ras [23], I analyzed the spatiotemporal dynamics of RBD_{Raf1}-GFP. I observed that the Ras-GTP-enriched domain translocated rotationally along the cell membrane as a traveling wave in control cells under confocal microscopy (Fig. 6A). The traveling wave was continuous for at least 30 min, as seen in the kymograph (Fig. 6B), with a mean domain size comparable to that reported previously (Fig. 6C) in 93% of control cells (Fig. 6D). On the other hand, the traveling wave was suppressed in fendiline-treated cells (Fig. 6A). In this case, the Ras-GTP-enriched domain occasionally formed but disappeared usually within 1 min (Fig. 6B), and the domain size and amplitude of the Ras-GTP enrichment were smaller than in control cells (Fig. 6C). Although some cells exhibited the traveling wave continuously, the fraction of such cells was reduced to 4% (Fig. 6D). Additionally, 57% of fendiline-treated cells exhibited transient dynamics, and no domain was observed during the 30-min observation in 39% of cells. The frequency of domain formation was reduced also in the absence of caffeine, suggesting that spontaneous firing was suppressed by fendiline (Fig. 6E) [20]. The traveling wave of PIP3/PTEN, which is driven by the traveling wave of Ras-GTP, was also suppressed in fendiline-treated cells (Fig. 6F, 6G, 6H). Overall, the fact that the traveling wave was suppressed by fendiline demonstrates that the excitability of Ras was suppressed by the drug.

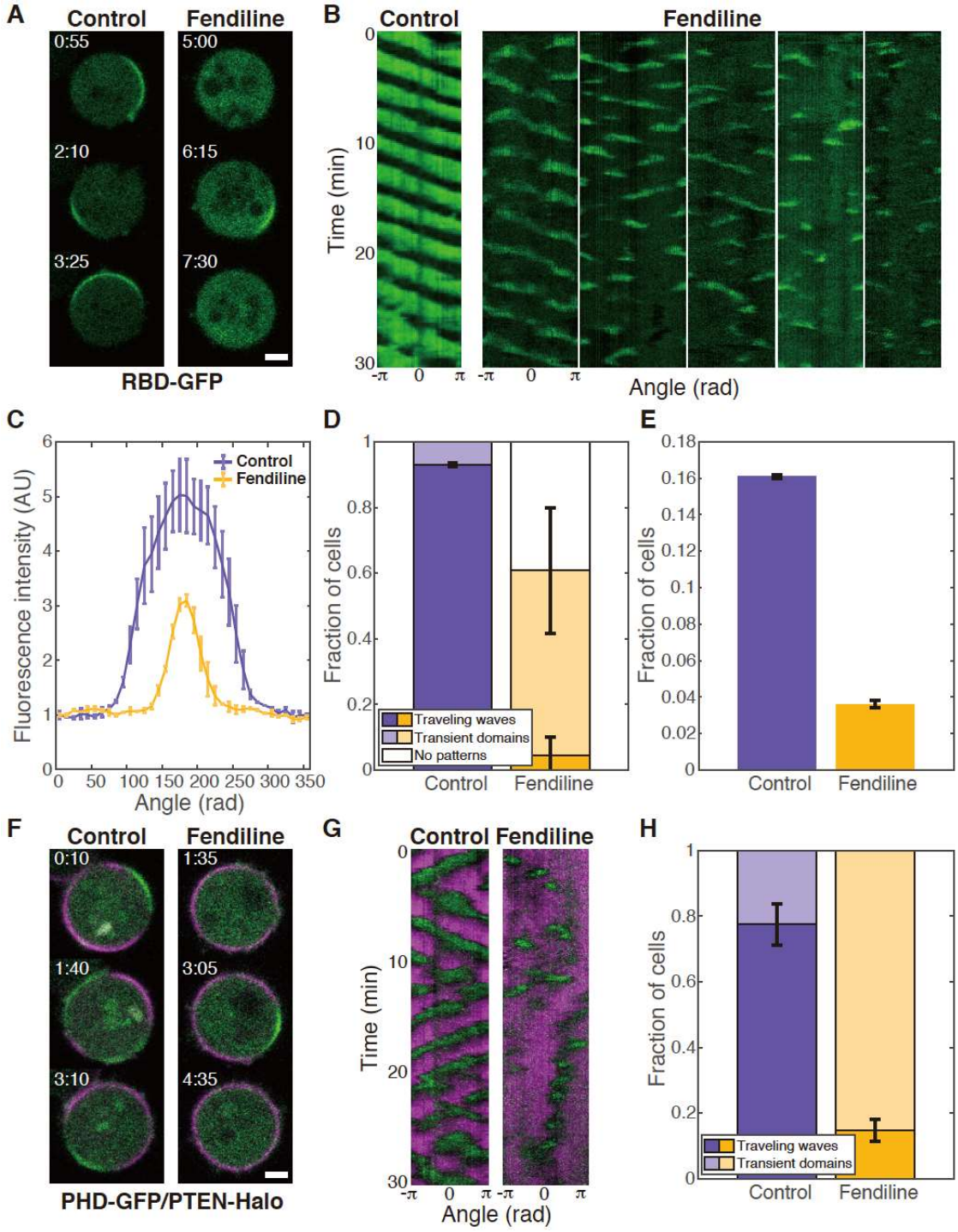


Figure 6. The excitability of Ras-GTP was suppressed by fendiline.

(A-E) The excitability of Ras-GTP was suppressed by fendiline. (A-E) The dynamics of Ras-GTP. (A) Representative time-lapse images of cells expressing RBD_{Raf1}-GFP. (B) Representative kymographs of the fluorescence intensity on the cell membrane. (C) The fluorescence intensity distribution along the cell membrane. Control, n = 18 cells;

fendiline, n = 19 cells. (D) Fraction of cells showing traveling waves. P = 0.001 and 0.046 (control versus fendiline for traveling waves and transient domains, respectively) by Welch's t test. Control, n = 72 cells; fendiline, n = 121 cells. (E) Fraction of cells showing transient domain generation in the absence of caffeine. P = 0.004 (control versus fendiline). Control, n = 416 cells; fendiline, n = 421 cells. (F-H) The dynamics of PIP3/PTEN. (F) Representative time-lapse images of cells expressing $PHD_{PKB/Akt}$-GFP and PTEN-Halo. (G) Representative kymographs. (H) Fraction of cells showing traveling waves. P = 0.001 (control versus fendiline). Control, n = 120 cells; fendiline, n = 169 cells. Cells were treated with 5 μM latrunculin A and 4 mM caffeine unless noted otherwise. Scale bars, 3 μm. Time, min:sec. Error bars, SD.

3.3 The activation of Ras was suppressed by fendiline

To examine how the excitability was suppressed, the dynamics of excitation was analyzed by monitoring transient membrane localization of RBD_{Raf1}-GFP after the excitation was triggered externally with an addition of 3',5'-cyclic adenosine monophosphate (cAMP) (Fig. 7A) [20]. The fraction of control cells that showed the membrane localization increased dependently on cAMP concentration with a half-maximum response at 0.6 nM (Fig. 7B). In fendiline-treated cells, the dose-dependent curve was shifted rightward with a half-maximum response at 4.0 nM, suggesting that the excitation occurred less effectively in these cells than in control cells. The amount of RBD_{Raf1}-GFP that translocated to the cell membrane was smaller in fendiline-treated cells than in control cells (Fig. 7A): the fluorescence intensity in the cytosol was reduced by up to 40% in control cells, but only up to 20% in fendiline-treated cells that showed excitation (Fig. 7C). Even at the maximal response of excitation, the spatial distribution of RBD_{Raf1}-GFP across the cell membrane was heterogenous in fendiline-treated cells. These results suggest that fendiline suppressed positive feedback-mediated Ras activation for locally amplifying Ras-GTP to cross the threshold of the excitation and spatially spreading the excited state to nearby membrane.

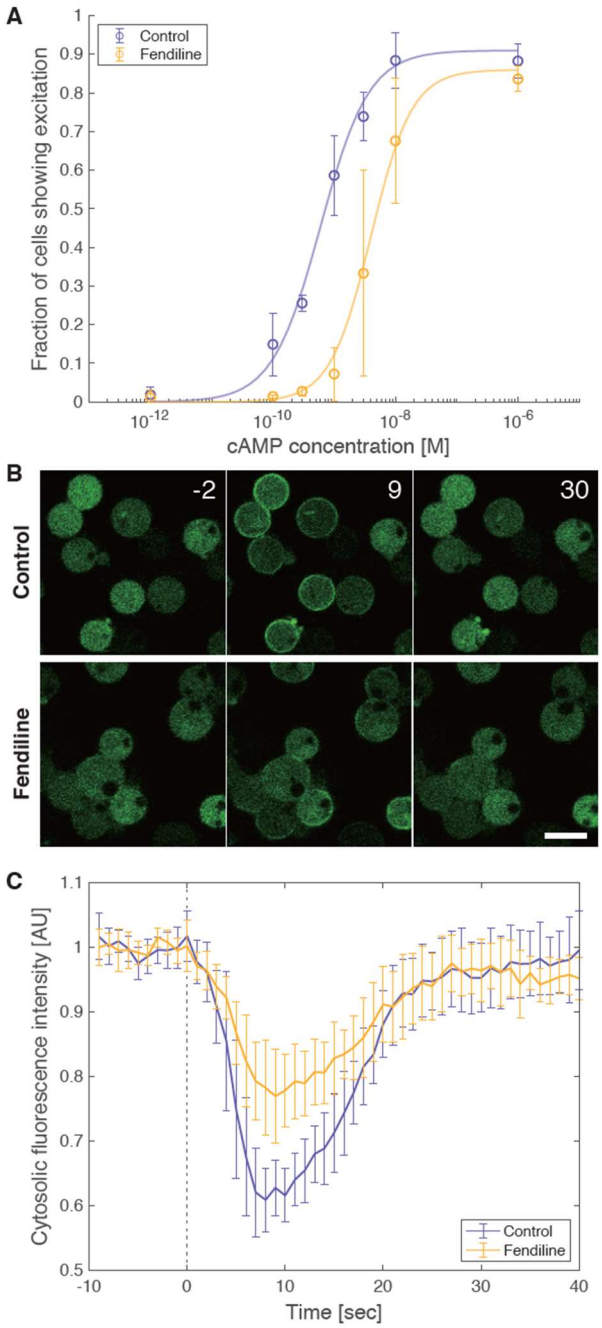


Figure 7. The activation of Ras was suppressed by fendiline.

(A) Dose dependence curve of the fraction of the cells that exhibited excitation upon the uniform simulation with cAMP. The data shows a mean and SD of 3 independent experiments and fitted to an equation, $F(x) = min + (max - min)\frac{x^h}{x^h + K^h}$, with h = 1.1 (control) and 1.3 (fendiline). (B) Time-lapse images of the cell before and after the stimulation with 3 nM cAMP. (C) The fluorescence intensity in the cytoplasm

quantified in (B). The data shows a mean and SD of 10 cells that exhibited the excitation. Scale bar, 3 μm. Time, sec.

3.4 Traveling waves were not recovered by an over-expression of Ras

To test if an amount of Ras was insufficient for the positive feedback in fendiline-treated cells, the expression level was examined in the cell lysate by western blotting with anti-Pan-Ras antibody, which has been known to detect RasG (Fig. 8A) [41]. The quantification of the bands derived from the equal numbers of cells showed that the amount of RasG in fendiline-treated cells was approximately 78% of that of control cells (Fig. 8B). Assuming that the control and fendiline-treated cells were spheres with the radius of 5.0 mm and 4.5 mm, which were mean values measured in the confocal images, respectively, it is estimated that the concentration of RasG in the individual cells was not changed drastically after the treatment (Fig. 8C). In addition, an over-expression of RasG could not recover the loss of traveling waves: RasG-over-expressing cells after the cultivation with fendiline showed the excitation more frequently, but the Ras-GTP-enriched domain usually disappeared rapidly and hardly propagated as a traveling wave (Fig. 8D, 8E, 8F). These results suggest that while the local amplification of Ras-GTP can be enhanced by an excess amount of Ras, it was not sufficient for spatially spreading the excited state, which likely require other mechanism than an availability of Ras.

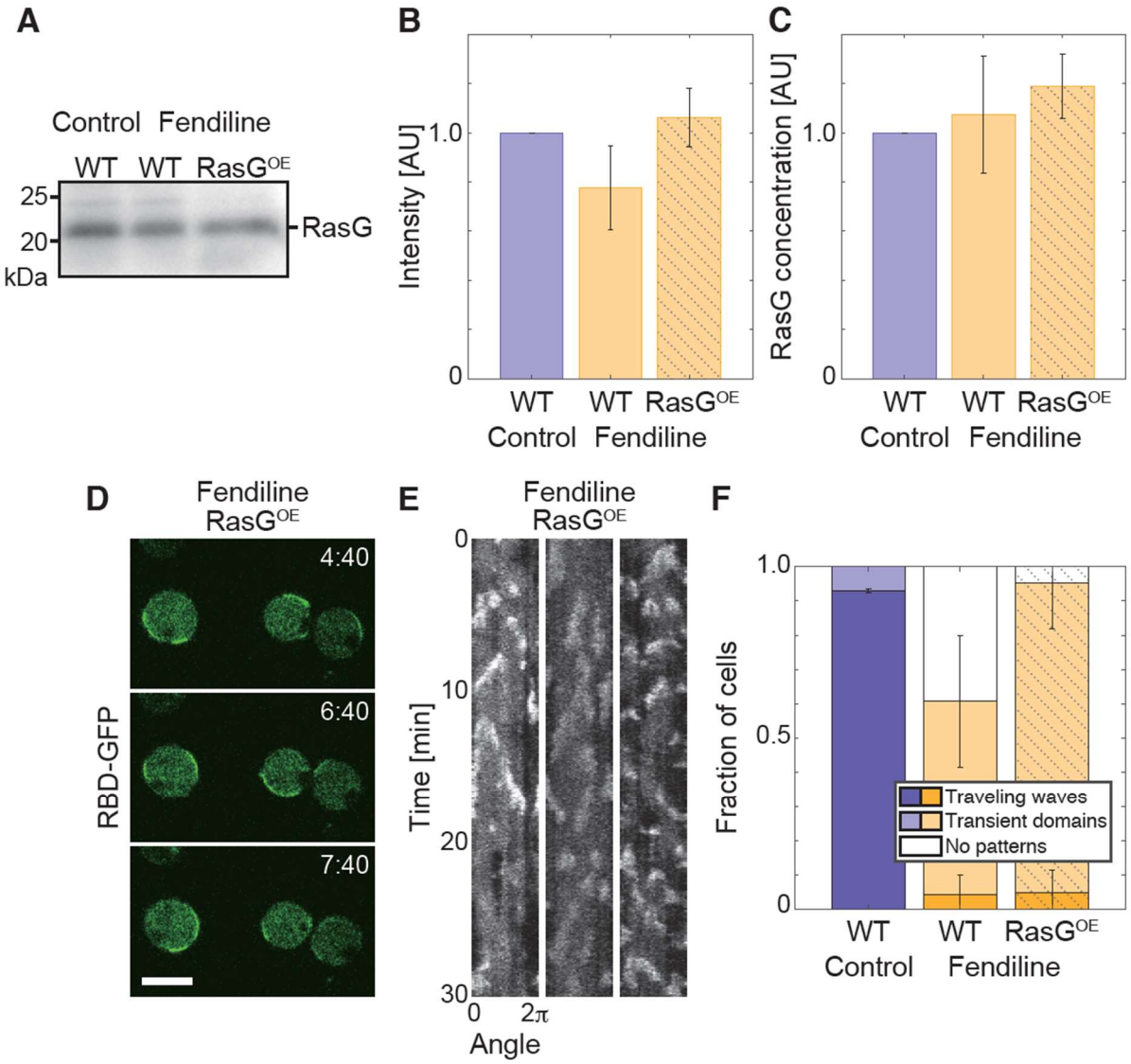


Figure 8. The expression of RasG was not significantly changed by fendiline and not the cause for the suppression of the traveling wave.

(A-C) Quantification of the expression of RasG. (A) Western blot of RasG detected with anti-Pan-Ras antibody in whole cell lysate from an equivalent numbers of cells. (B) Quantification of the band intensity in (A). (C) RasG concentration estimated by normalizing the band intensity by cell volume. The mean cell volume was estimated by assuming the cells as spheres with the radius measured in the confocal images of latrunculin A-treated cells (Fig. S2). (D-F) Dynamics of Ras-GTP in cells over-expressing RasG. (D) Representative images of RBDRaf1-GFP in cells over-expressing RasG. Scale bar, 10 μm. Time, min:sec. (E) Representative kymographs of RBD_{Raf1}-GFP intensity measured on the cell membrane. (F) Fraction of cells showing traveling waves. The means and SDs are shown (control, WT, same as Fig. 2D; fendiline, WT,

same as Fig. 2D; fendiline, RasG^{OE}, n = 29 cells).

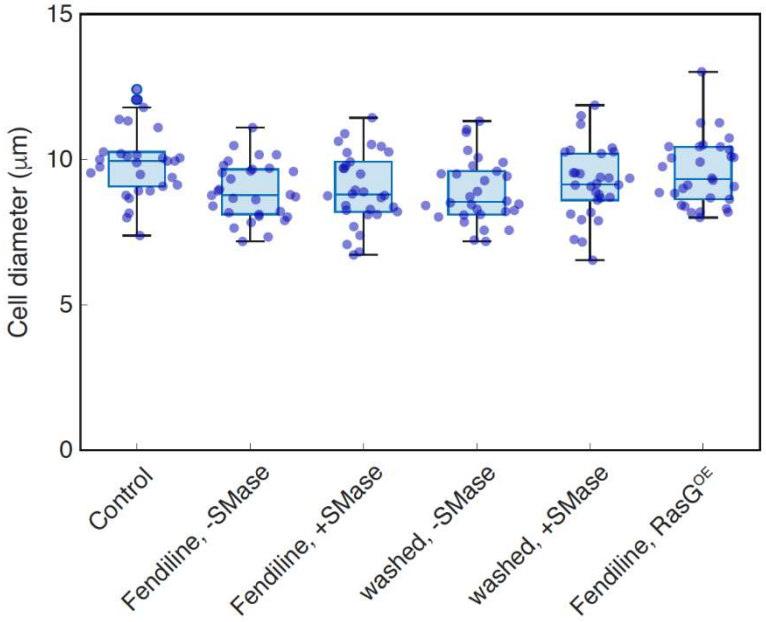


Figure 9. Cell diameters.

Cell diameters were measured in the images acquired under confocal microscopy in the presence of latrunculin A.

3.5 Traveling waves were recovered by eliminating accumulated SM or supplementation with PS

To test if the traveling wave was lost due to the abnormality of SM on the cell membrane, I firstly examined the SM level by staining with Lysenin (Fig. 10A, 10B) [42][43]. The cells were fixed with paraformaldehyde and glutaraldehyde, permeabilized with Triton X-100, and incubated with mCherry-Lysenin. In control cells that were cultivated for 48 hours in the medium and starved for 3 hours in phosphate buffer both in the presence of DMSO, the fluorescence was detected on the cell membrane as well as intracellular membranes (Fig. 10A, “Control, -SMase”). By treating the cells with extracellularly added SMase during the starvation [28], the fluorescence intensity on the cell membrane was decreased (Fig. 10A, 10B, “Control, +SMase”). It suggests that the amount of Lysenin most likely reported the SM level in D. discoideum cells. The intensity was higher in the cells cultivated and starved in the presence of fendiline than in the absence (Fig. 10A, 10B, “Fendiline, -SMase”), which was also decreased by the treatment with externally added SMase during the starvation (Fig. 10A, 10B, “Fendiline, +SMase”). Therefore, it is most likely that fendiline caused SM accumulation on the cell membrane via the inhibition of SMase.

Next, I examined whether reducing the amount of SM restores the Ras excitability in fendiline-treated cells. After 48 hours of cultivation and 3 hours of starvation, SMase addition, fendiline removal, or both were performed upon the cells prepared for microscopic observation in the presence of fendiline. The amount of SM quantified with mCherry-Lysenin was reduced to 51-88% after 30 min of these treatment, and the degree of reduction was more pronounced with fendiline removal, performed by buffer exchange (“washed” in Fig. 10), than with SMase addition and was greatest for both (Fig. 10C, 10D). Concomitantly, the traveling wave appeared in these cells, and the fraction of cells showing traveling wave was increased from 19% to 68-90% depending on the degree of SM reduction (Fig. 10E, 10F, 10G). The kymographs revealed that the spatiotemporal dynamics of the traveling waves regained in the fendiline-treated cells by the means of SM reduction were quite similar to those of control cells (Fig. 10F). Neither SMase addition nor fendiline removal affected RasG expression within 30 min

(Fig. 10H). These results suggest that the traveling wave of Ras-GTP is suppressed due to abnormally accumulated SM on the cell membrane.

Since the abnormal SM metabolism is known to cause a depletion of PS from cell membranes in mammalian cells, we further examined whether an external addition of PS can also recover the traveling wave in fendiline-treated *D. discoideum* cells [28]. PS dissolved with BSA in phosphate buffer was added to the cells after 48 hours of cultivation and 3 hours of starvation in the presence of fendiline. Within 60 min after the addition, the traveling wave of RBD_{Raf1}-GFP appeared in 49% of the cells (Fig. 11). Such recovery was not observed by BSA only, suggesting that the traveling wave was triggered by PS. In addition, with the cells showing transient domain generation included, 81% of fendiline-treated cells exhibited self-organization of Ras-GTP-enriched domain after addition of PS, contrasting to 48% after the addition of BSA (Fig. 11C). Attempts to monitor PS level using a fluorescent probe such as LactC2 failed because this probe hardly localized to the cell membrane in *D. discoideum* cells under our experimental conditions [44]. Therefore, though the subcellular localization of the incorporated PS is still unclear, it is possible that PS positively regulates the excitability of Ras.

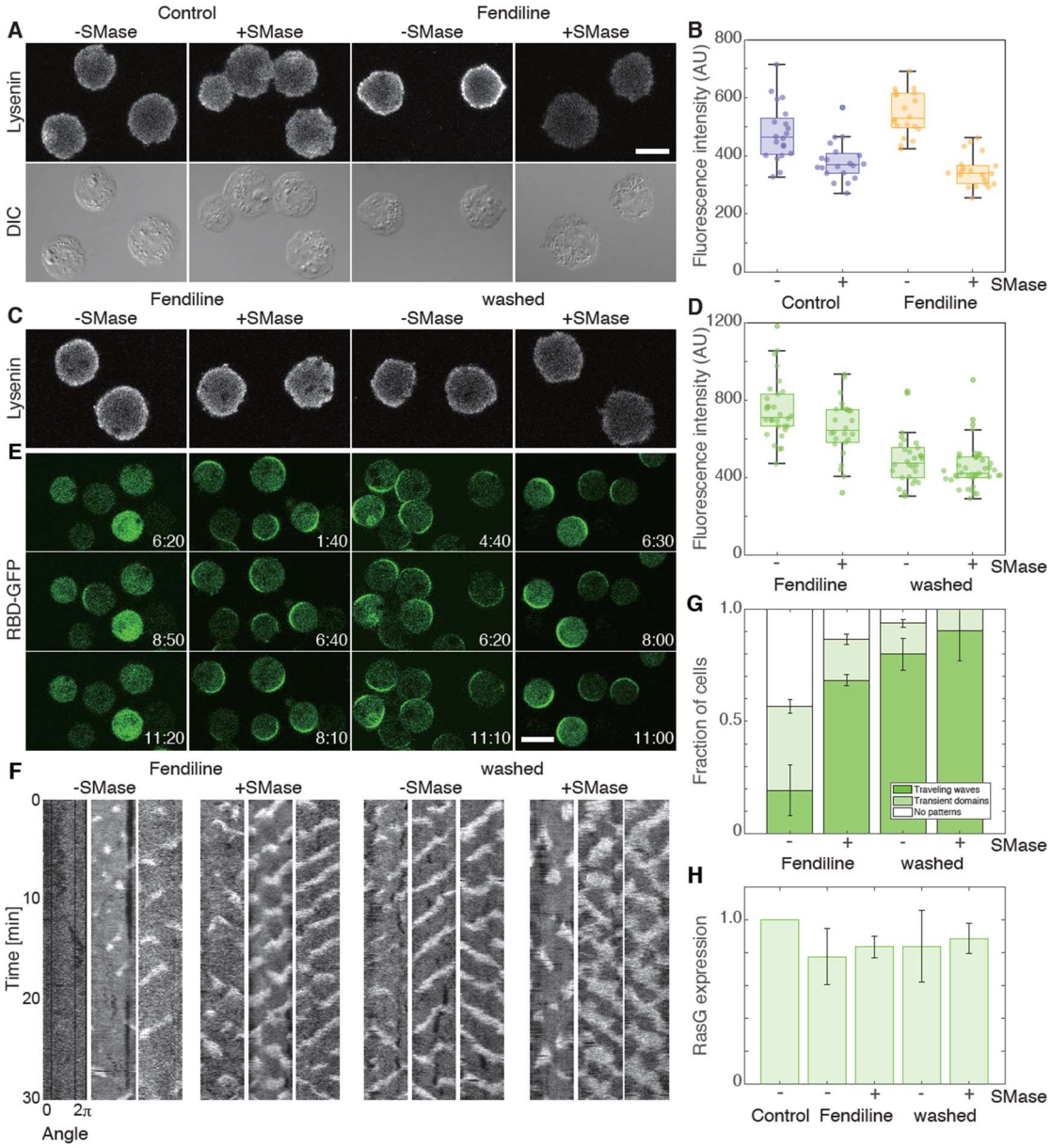


Figure 10. Recovery of Ras-GTP traveling waves by the elimination of SM accumulated on the cell membrane.

(A, B) Imaging analysis of SM levels with m-Cherry-Lysenin. (A) Representative images of mCherry-Lysenin in control ("Control") and fendiline-treated ("Fendiline") cells starved in the absence ("-SMase") and presence ("+SMase") of SMase. (B) Quantification of the fluorescence intensity on the cell membrane in (A). (C, D) Elimination of accumulated SM in fendiline-treated cells. (C) Representative images of mCherry-Lysenin in fendiline-treated cells 30 min after SMase addition ("Fendiline, +SMase"), fendiline removal ("washed, -SMase") or both ("washed, +SMase"). (D)

Quantification of the fluorescence intensity on the cell membrane in (C). (E-G) Recovery of Ras-GTP traveling waves in fendiline-treated cells. (E) Representative images of RBD_{Raf1}-GFP in fendiline-treated cells 30 min after the indicated treatments. Time, min:sec. (F) Representative kymographs of RBD_{Raf1}-GFP intensity measured on the cell membrane. (G) Fraction of cells showing traveling waves and transient domains. The means and SDs are shown (Fendiline, -SMase, n = 39 cells; Fendiline, +SMase, n = 32 cells; washed, -SMase, n = 52 cells; washed, +SMase, n = 37 cells). (H) Quantification results of RasG detected with anti-Pan-Ras antibody in whole cell lysates from an equivalent numbers of cells. Scale bars, 10 μm.

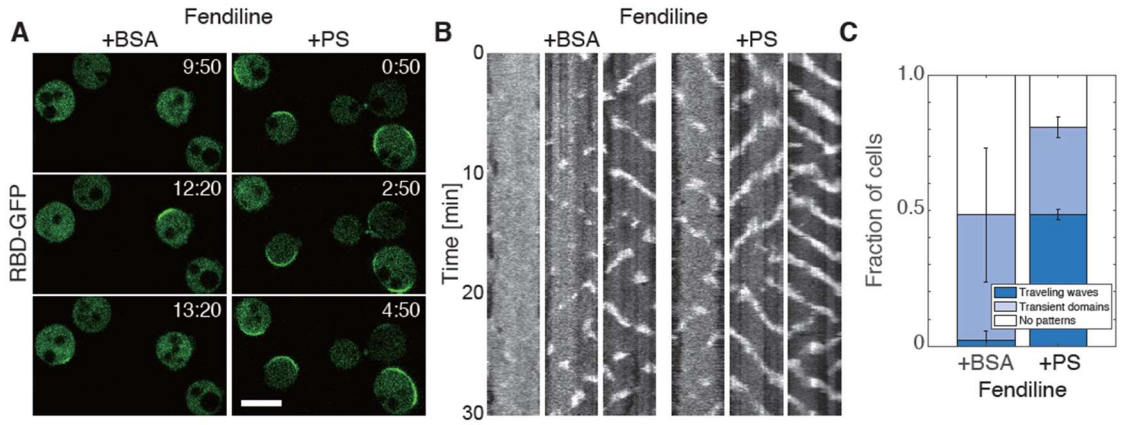


Figure 11. Recovery of Ras-GTP traveling waves by exogenous PS.
(A) Representative images of RBD_{Raf1}-GFP in fendiline-treated cells incubated with BSA or PS. Scale bar, 10 μm. Time, min:sec. (B) Representative kymographs of RBD_{Raf1}-GFP intensity measured on the cell membrane. (C) Fraction of cells showing traveling waves and transient domains. The means and SDs are shown (BSA, n = 43 cells; PS, n = 37 cells).

3.6 Cell motility required sphingomyelin metabolism

The defect of Ras excitable system caused by SMase inhibition was examined in the absence of latrunculin A, where the cells exhibit spontaneous cell migration [45]. The cells cultivated in the control media showed elongated shape with a clear anterior-posterior morphological polarity and migrated spontaneously in random directions with an average migration speed of 11.1 $\pm$ 4.5 μm/min (n = 196 cells) (Fig. 12A, 12B, 12G). The cells cultivated in the presence of fendiline showed less elongated shape and migrated less effectively with an average migration speed of 5.6 $\pm$ 2.8 μm/min (n = 113 cells). With SMase addition, fendiline removal or both, fendiline-treated cells spontaneously acquired the cellular morphological polarity and motility, depending on the degree of SM elimination (Fig. 12C, 12D, 12G). The recovery was also achieved with PS addition, but not with RasG overexpression (Fig. 12E, 12F, 12G). BSA was able to restore some motility, which was likely due to RasG-independent process such as cell-substrate adhesion signaling modulated by coating the glass surface with BSA, but PS had an additive effect to it. These results suggest that the Ras excitable system offers a mechanism for spontaneous generation of cell polarity and motility depending on the SM and PS metabolism.

D. discoideum cells show chemotaxis to cAMP, which I quantitatively analyzed by applying a micropipette releasing cAMP among the cells. The control cells moved chemotactically with different degrees of directedness and speed depending on their distance from the tip of the micropipette (Fig. 13A, 13B, 13F). When located far from the micropipette, control cells often moved in the direction opposite of the chemoattractant source but finally moved up the gradient after frequent directional changes. On the other hand, fendiline-treated cells failed to show such biased motility when located far from the micropipette (Fig. 13C, 13D, 13F). Importantly, such stochasticity-driven chemotaxis under the shallow gradient was restored by either SMase addition, PS addition or fendiline removal (Fig. 13E, 13F, 14). These results suggest that under a shallow and low concentration gradient, the chemotactic motility was largely dependent on the basal motility offered by Ras excitable system with an aid of proper levels of SM and PS on the cell membrane.

Additionally, I noticed that the cells became smaller and the doubling time was increased to 20 hours from 16 hours when the cells were cultured in the presence of

fendiline. Therefore, multiple cellular functions involving symmetry breaking by Ras were consistently affected by fendiline, suggesting an essential role of SM metabolism in regulating Ras excitability.

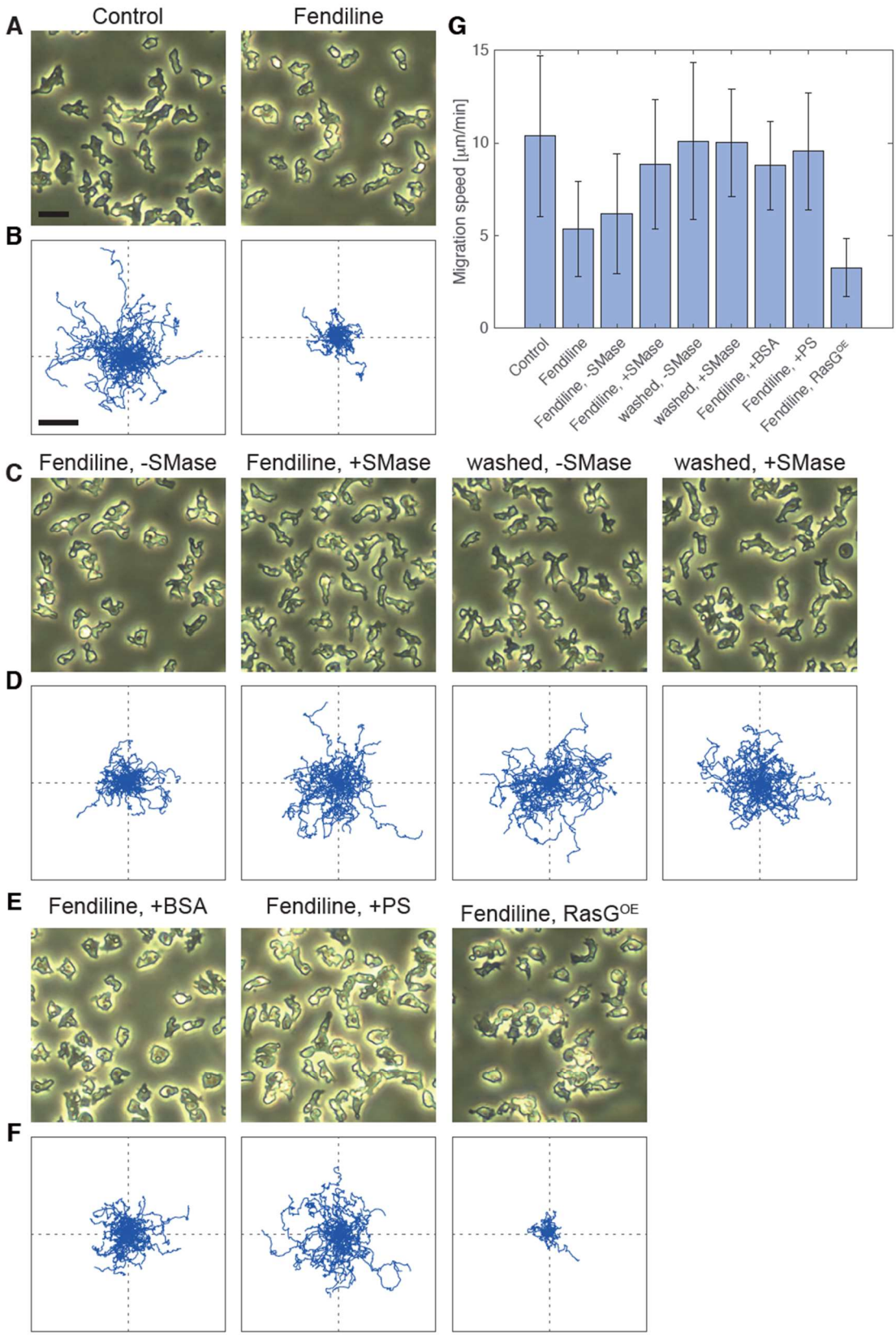


Figure 12. Spontaneous cell migration was suppressed by fendiline, which was

recovered by an external addition of SMase or PS as well as fendiline removal. (A, C, E) Representative images of the cells. Scale bar, 20 μm. (B, D, F) Migration trajectories of the cells for 30 min. Scale bar, 100 μm. (G) Migration speed. The means and standard deviations are shown (Control, n = 130 cells; fendiline, n = 90 cells; fendiline, -SMase, n = 71 cells; fendiline, +SMase, n = 95 cells; washed, -SMase, n = 104 cells; washed, +SMase, n = 84 cells; fendiline, +BSA, n = 75 cells; fendiline, +PS, n = 73 cells; fendiline, $RasG^{OE}$, n = 44 cells).

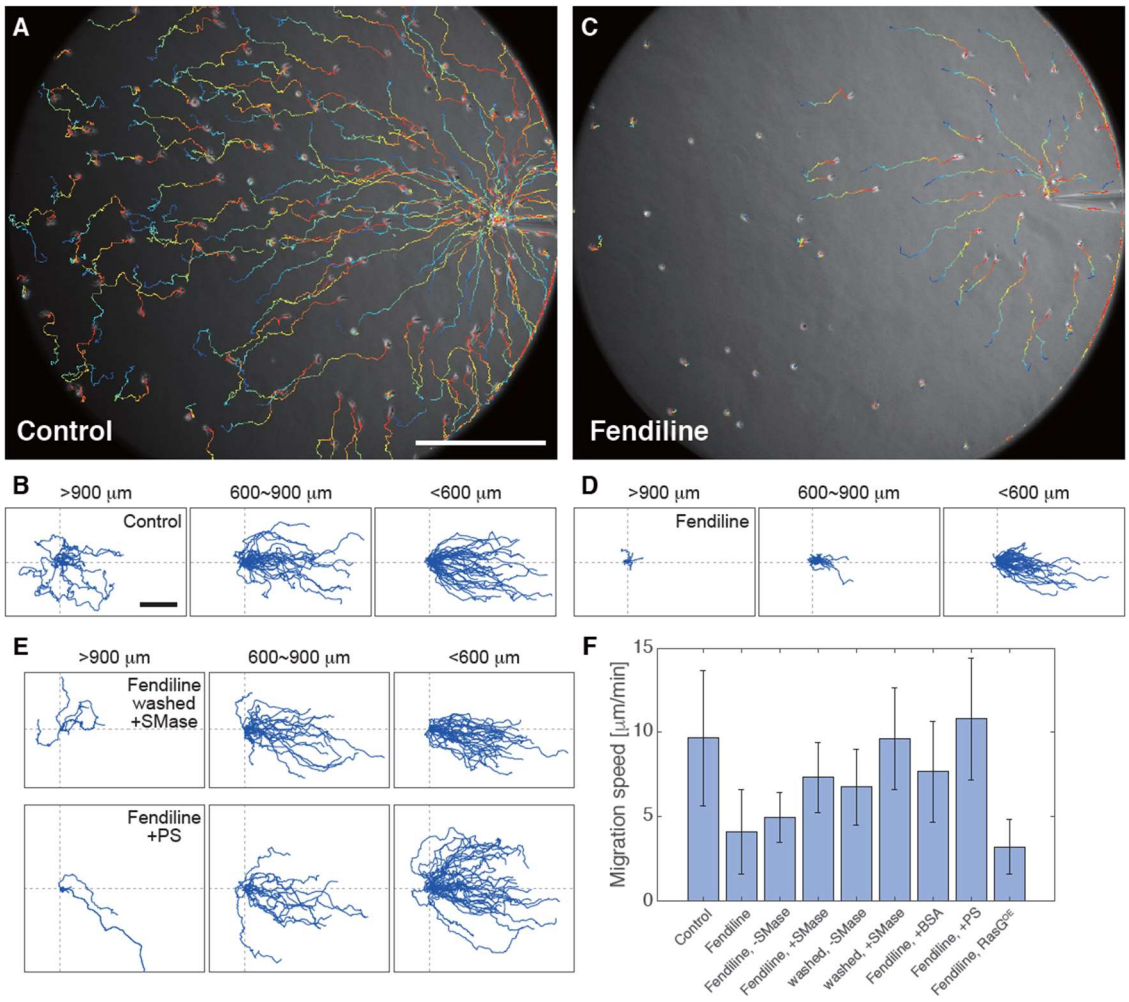


Figure13. Chemotaxis under a shallow chemical gradient was suppressed by fendiline, which was recovered by an external addition of SMase or PS as well as fendiline removal.

(A, C) Representative migration trajectories of control (A) and fendiline-treated cells (C) for 30 min after releasing 100 nM cAMP from a micropipette. The color code indicates the time after the gradient application, where a hotter color indicates a later time. (B, D, E) Migration trajectories for 30 min of control (B) and fendiline-treated cells (D, E). The cells were located >900 (left), 600~900 (center) and <600 μm (right) from the micropipette tip. (F) Migration speed. The means and standard deviations are shown (Control, n = 217 cells; fendiline, n = 130 cells; fendiline, -SMase, n = 79 cells; fendiline, +SMase, n = 79 cells; washed, -SMase, n = 57 cells; washed, +SMase, n = 98 cells; fendiline, +BSA, n = 104 cells; fendiline, +PS, n = 94 cells; fendiline, RasGOE, n = 80 cells). Scale bars, 100 μm.

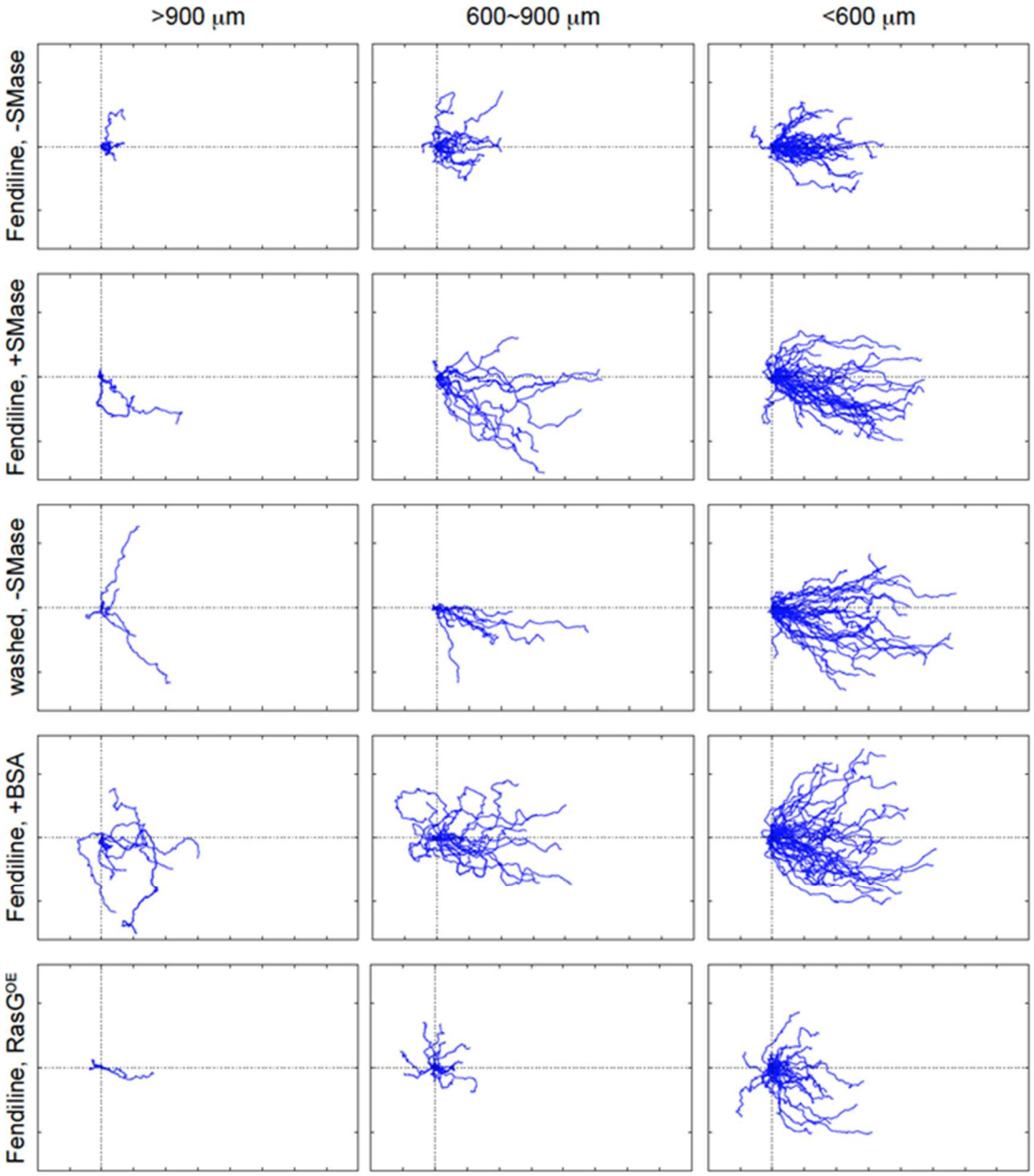


Figure 14. Chemotaxis under a shallow chemical gradient was suppressed by fendiline. (continued from Figure. 13).

Representative migration trajectories of fendiline-treated cells with indicated manipulations.

3.7 Conditions of fixation

Because there was no common protocol for *D. discoideum* in this laboratory for single molecule localization of Ras-GTP by PALM using mKikGR-tagged RBD_{Raf1} (RBD_{Raf1}-mKikGR), it was necessary to set a common protocol.

First, it was necessary to find the condition of the cell fixation. Fixation of cells is the critical first step for investigations. To observe single molecule with different fixation conditions, it was examined by the conditions with references [46][47][48][49].

The conditions and method are as follows. After fixation, it was determined if these two are maintained or not as evaluation contents.

D. discoideum cells had a developmental cycle that was initiated to survive starvation, and which relied heavily upon chemotaxis. During development cycle, for the cell to move, it had to extend a pseudopod at the front of the cell and retract at the rear of the cell. In this process, cells have a characteristic shape.

It was performed of 17 fixative conditions, two conditions were maintained of cell shape and RBD localization were maintained (Table 1. 3.7% FA in MeOH, - 20 °, 30 sec, 3.7% FA in DB buffer, 14 min 30 sec, r.t. and 4% PFA + 0.25 % GA, 0.1% triton, 10 min, r.t.). Because of importance of the maintenance of the cell membrane lipid bilayer, it was selected the fixation method avoiding the organic solvent.

Conditions of fixation	Cell shape	Protein localization
① 3.7% FA in MeOH, - 20	O	X
② 3.7% FA in MeOH, - 20 °, 30 sec, 3.7% FA in DB buffer, 14 min 30 sec, r.t.	O	O
③ 3.7% FA in MeOH, - 20 °, 30 sec, 3.7% FA in PDF buffer, 14 min 30 sec, r.t.	O	X
④ MeOH, - 20 °, 30 sec	X	X
⑤ MeOH, - 20 °, 1 min	O	X
⑥ 4% PFA, 10 min, r.t.	X	X
⑦ 4% PFA, 30 min, r.t.	X	X
⑧ 4% PFA + 0.1 % GA, 30 min, r.t.	X	X
⑨ 4% PFA + 0.2 % GA, 30 min, r.t.	X	X
⑩ 4% PFA + 0.25 % GA, 0.1 % triton, 10 min, r.t.	O	O
⑪ 4% PFA + 0.25 % GA, 0.1 % triton, 10 min, r.t.	O	X
⑫ 4% PFA, 15 % picric acid, 0 mM sucrose in PIPES buffer, 30 min, r.t.	X	X
⑬ 4% PFA, 15% picric acid, 62.5 mM sucrose in PIPES buffer, 30 min, r.t.	X	X
⑭ 4% PFA, 15% picric acid, 125 mM sucrose in PIPES buffer, 30 min, r.t.	X	X
⑮ 4% PFA + 0.25% GA, 0 mM sucrose in HL5, 10 min, r.t.	X	X
⑯ 4% PFA + 0.25% GA, 125 mM sucrose in HL5, 10 min, r.t	X	X
⑰ 4% PFA + 0.25% GA, 250 mM sucrose in HL5, 10 min, r.t.	X	X

Table 1. Conditions of fixation

FA, formaldehyde; PFA, paraformaldehyde; GA, glutaraldehyde; PDF buffer (development buffer), 1.5 g KCl, 1.6 g K_2HPO_4, 1.8 g KH_2PO_4 per L, buffered to pH6.5 with KOH; MeOH, methanol; PIPES buffer, Piperazine-1,4-bis(2-ethanesulfonic acid) (PIPES) 20 mM buffered to pH 6.0 with NaOH.

3.8 Fendiline reduced the numbers of Ras-GTP molecules and clusters

I investigated the single molecule localization of Ras-GTP by PALM using mKikGR-tagged RBD_{Raf1} (RBD_{Raf1}-mKikGR) [50]. The *x* and *y* coordinates of RBD_{Raf1}-mKikGR molecules bound to the membrane in fixed cells showed that the molecules distributed more sparsely in fendiline-treated cells (Fig. 15A, 15B; Fig. 15). The number density, which is the total number of molecules divided by the area of the membrane, was 38.7 $\pm$ 10.8 molecules/μm^2 (n = 16 cells) in fendiline-treated cells compared to 56.9 $\pm$ 16.1 molecules/μm^2 in control cells (n = 14 cells) (Fig. 15C). A quadrat analysis showed that the local number density, which is the number of molecules present in an arbitrary region of a square with 300 nm lengths, followed the sum of two statistical distributions (Fig. 15D, insets). The smaller mean distribution showed a relationship in which the variance approximately equaled the mean, indicating a random point pattern, whereas the larger mean distribution showed a relationship in which the variance was greater than the mean, indicating a clustered point pattern (Fig. 15D) [51]. These observations suggest that there were at least two local regions within each cell: a region where the molecules randomly distributed at a lower density and a region where they showed clustering at a higher density. The mean and variance values of the local number density outside the clusters were obviously reduced by fendiline.

Ripley's K function revealed a positive peak at about 200 nm irrespective of fendiline treatment, indicating that a characteristic radius of the cluster was about 200 nm (Fig. 15E) [52]. Hierarchical clustering was performed for the data of each cell to group individual molecules into clusters at an arbitrary Euclidean distance. At the distance 200 nm, the number of clusters containing more than 5 molecules in a single cell was smaller on average with fendiline treatment than without (Fig. 15F). Consistently, these clusters distributed more sparsely with fendiline treatment (Fig. 15G, 15H). The Hopkins-Skellam index, which equals 1 for a random distribution, less than one for a dispersed distribution, and greater than 1 for a clustered distribution, indicated that the centroids of the clusters distributed in a somewhat dispersed manner in control cells (Fig. 15I) [53]. However, fendiline attenuated the propensity to show a dispersed distribution. Therefore, the local number density of Ras-GTP molecules is likely to be related to the efficiency of clustering and reduced by fendiline due to the suppression of activation even in the resting state cells.

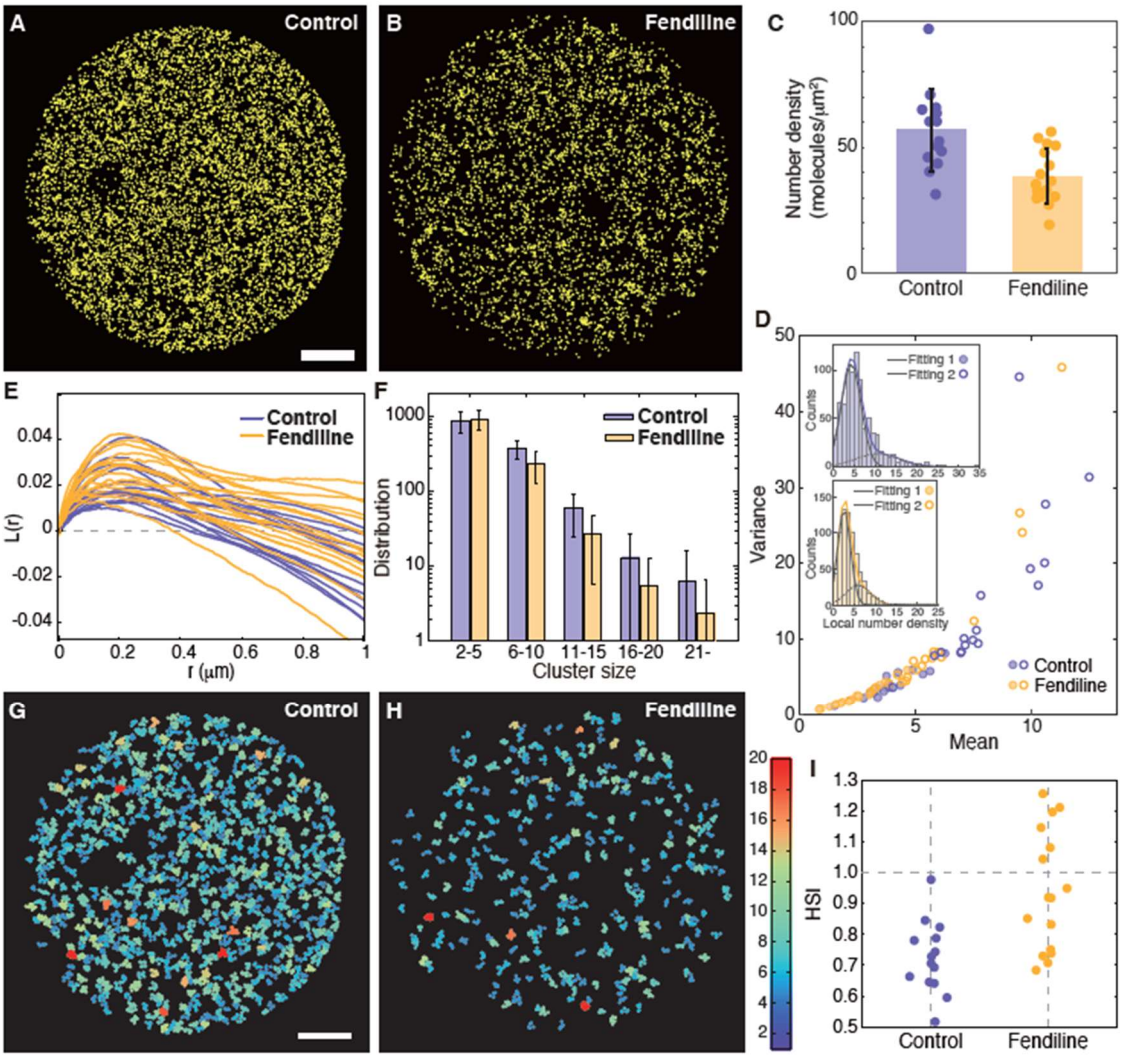


Figure 15. The number densities of Ras-GTP molecules and clusters were reduced by fendiline.

(A-F) Spatial analysis of individual Ras-GTP molecules. (A, B) Representative images showing single-molecule localization of RBD_{Raf1}-mKikGR in control (A) and fendiline-treated cells (B). (C) The number density of RBD_{Raf1} molecules in individual cells. P = 0.002 (control versus fendiline) by Welch's t test. (D) A variance vs. mean plot of the local number density. Statistical distribution of the local number density of RBD_{Raf1} molecules measured in a square area of 90,000 nm^2 was fitted with a sum of two Gaussian functions to obtain the means and variances (insets). (E) Ripley's K function calculated for individual cells. (F) The cluster size distribution. The mean and standard deviation of 14 control and 16 fendiline-treated cells are shown in (C, F). (G, H) A spatial analysis of individual Ras-GTP clusters. Images showing the position of molecules grouped to the clusters with a cluster size larger than 5 in (A, B). The cluster

size is indicated by color coding. (I) The Hopkins-Skellam index calculated for individual cells. Scale bars, 2 μm. Error bars, SD.

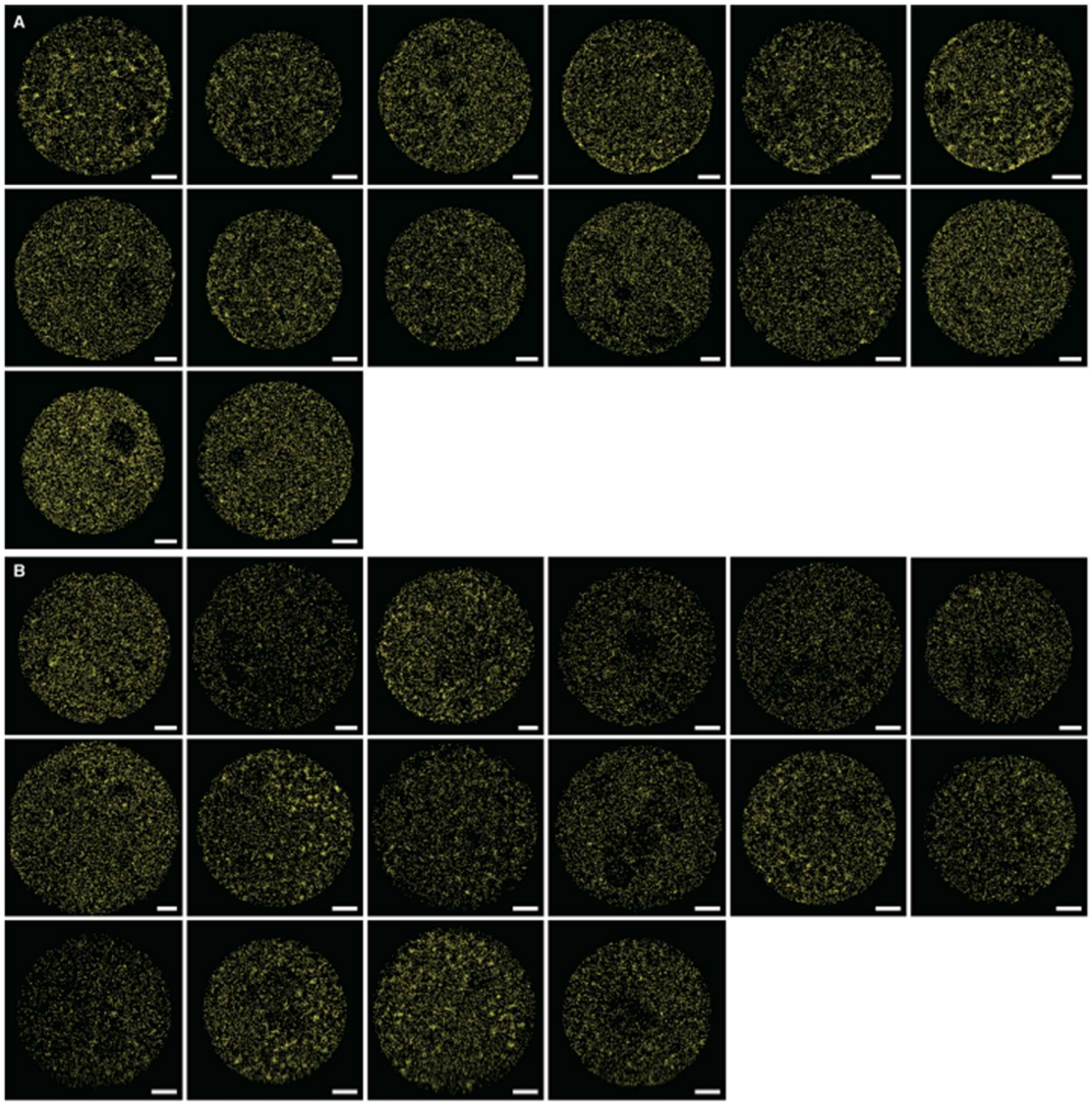


Figure 16. Gallery of PALM images.

(A) Control cells. (B) Fendiline-treated cells. Scale bars, 2 μm.

Discussion

In this study, super-resolution microscopy was used to quantify the signal and noise as a form of the mean and variance of the local number density of Ras-GTP molecules fluctuating spatially on the cell membrane. It was revealed that the excitability of Ras is supported by an appropriate magnitude of molecular noise generated through normal SM metabolism on the cell membrane. SM metabolism was necessary for the activation of Ras [29]. Here, I propose that the increase in the number density of Ras-GTP leads to the transient cluster formation, which probably offer the regulation mechanism of the excitation in the spontaneous generation of the anterior-posterior polarity in eukaryotic motile cells.

SM metabolism probably offered an optimal membrane environment for Ras in the excitable system. In the fendiline-treated *D. discoideum* cells, Ras could not be effectively activated by the stimulation with cAMP, and the number density of Ras-GTP molecules was constitutively reduced consequently resulting in the suppression of clustering. It is possible that a common regulation mechanism of Ras containing the C-terminal anchor sequence through SM metabolism shared among eukaryotic cells including K-Ras in mammalian cells and RasG and RasC in *D. discoideum*. It is required to quantitatively analyze the consequences of the blockade in the membrane lipid compositions in *D. disoideum* cells by biochemical measurement and cell imaging with fluorescently labeled probes specific for SM and PS like Lysenin and LactC2, respectively. The characteristic radius of the cluster has been reported to be ~20 nm for K-Ras and was estimated to be ~200 nm for Ras in *D. discoideum* cells, both of which was unaffected by the treatment with fendiline or other aSMase inhibitors [29]. It has been reported that K-Ras cluster is formed independently of cholesterol, that is, the clus ter is most likely different from lipid microdomains such as rafts [27][54].

Therefore, the mechanistic link between the aberrant SM metabolism and the suppression of Ras activation is probably independent of the structure of the lipid microdomains. Rather, as already reported, it is possible that the SM metabolism might be necessary to adjust the membrane lipid conditions, such as PS level in the cell membrane, for the retention of enough Ras molecules for the activation and cluster formation on the cell membrane via the interaction with its C-terminal anchor sequence [27][29]. The mechanism how the PS level is maintained under the normal SM metabolism has yet to be solved, but it is suggested that the excess SM causes an internalization of PS and that SM level controls the phospholipid asymmetry in the cell membrane [55][56][57]. Such mechanisms may be conserved among the eukaryotic

cells, and the SM metabolism blockade similarly resulted in the loss of Ras-GTP molecules and the clusters as well in *D. discoideum* cells, leading to the suppression of Ras activation in the excitation.

This study has demonstrated that the excitation involves a mesoscopic structure such as the Ras-GTP cluster, the dimension of which is larger than the single molecule but smaller than the Ras-GTP-enriched domain. It is most likely that the cluster arises transiently due to the locally increased number density of Ras-GTP through lateral diffusion of the individual molecules. The clusters were prominent within the Ras-GTP-enriched domain, but they were not excluded outside the domain, suggesting that the efficiency of clustering is regulated via the number density of the molecules. It further suggests that the clustering is not necessary the result of the excitation, but it is possible that the cluster provides a structural basis for the excitation. At the onset of an excitation, positive feedback amplifying the signal is triggered when the signal crosses the threshold due to the noise. The probability of the threshold-crossing depends on both the difference between the mean signal level and the threshold and the magnitude of the noise. Under a given threshold and noise magnitude, the probability is increased when the mean signal level is increased. Thus, an increased probability can be expected by locally accumulating molecules into the cluster. It should be noted that it remains unclear whether a single cluster composed of a relatively large number of Ras-GTP molecules is sufficient for triggering the excitation. Therefore, although it has been proposed that the physiological role of the Ras cluster is to maximize the gain of signaling with reducing the noise in mammalian cells [36][37][58][59], the Ras clusters in the excitable system of the motile cells play a role in enhancing the noise to effectively trigger the excitation. These results shed light on a novel role of these lipid species outside the microdomain to modulate the molecular noise utilized for the intrinsic dynamics of cellular signaling.

The present study illustrates that the spontaneous generation of the cellular polarity signal is controlled by a stochastic resonance-like mechanism operating within a single cell, adding an example of a living system that uses noise at the molecular level.

References

1. **J. T. Bonner , D. S. Barkley, E. M.Hall, T. M. Konijn, J. W. Mason, G. O'Keefe, & P. B. Wolfe,** Acrasin, acrasinase, and the sensitivity to acrasin in *Dictyostelium discoideum. Developmental Biology*, **20(1)**, 72–87 (1969).
2. **J. T. Bonner,** The Pattern of Differentiation in Amoeboid Slime Molds. The American Naturalist, **86(827)**, 79–89 (1952).
3. **J. Sternfeld , C. N. David,** Fate and regulation of anterior-like cells in *Dictyostelium* slugs. *Developmental Biology*, **93(1)**, 111–118 (1982).
4. **P. N. Devreotes, P. L. Derstine, T. L. Steck,** Cyclic 3',5' AMP relay in *Dictyostelium discoideum*. I. A technique to monitor responses to controlled stimuli. *The Journal of Cell Biology*, **80(2)**, 291–299 (1979).
5. **M. C. Dinauer, S. A. MacKay, P. N. Devreotes,** Cyclic 3',5'-AMP relay in *Dictyostelium discoideum* III. The relationship of cAMP synthesis and secretion (1980).
6. **P. N. Devreotes and S. H. Zigmond,** Chemotaxis in Eukaryotic Cells: A Focus on Leukocytes and Dictyostelium., *Annu. Rev. Cell Biol*, **4**: 649-86 (1988).
7. **PJ. M. Van Haastert and M. Postma,** Biased RandomWalk by Stochastic Fluctuations of Chemoattractant-Receptor Interactions at the Lower Limit of Detection, *Biophys. J*, **93(5)**, 1787-1796 (2007).
8. **O. D. Weiner, W. A. Marganski, L. F. Wu, S. J. Altschuler, M. W. Kirschner,** An actin-based wave generator organizes cell motility. *PLoS biology*, **5(9)**, e221 (2007).
9. **J. S. King, R. H. Insall,** Chemotaxis: finding the way forward with *Dictyostelium*. *Trends in Cell Biology*, **19(10)**, 523-530 (2009).
10. **Y. Arai, T. Shibata, S. Matsuoka, M. J. Sato, T. Yanagida, M. Ueda**, Self-organization of the phosphatidylinositol lipids signaling system for random cell migration. *Proc. Natl. Acad. Sci. USA*. **107**, 12399-12404 (2010).
11. **C. Huang, M. Tang, C. Shi, P. Iglesias, P. N. Devreotes,** An excitable signal integrator couples to an idling cytoskeletal oscillator to drive cell migration. *Nat Cell Biol*. **15**, 1307-1316 (2013).
12. **D. Weiner, W. A. Marganski, L. F. Wu, S. J. Altschuler, M. W. Kirschner**, An actin-based wave generator organizes cell motility. *PLoS Biol*. **5**, e221 (2007).
13. **H. W. Yang, S. R. Collins, T. Meyer,** Locally excitable Cdc42 signals steer cells

during chemotaxis. *Nat Cell Biol*. **18**, 191-201 (2016).

14. **P. N. Devreotes, S. Bhattacharya, M. Edwards, P. A. Iglesias, T. Lampert, Y. Miao,** Excitable Signal Transduction Networks in Directed Cell Migration. *Annu Rev Cell Dev Biol.* **33**, 103-125 (2017).
15. **C. A. Parent, B. J. Blacklock, W. M. Froehlich, D. B. Murphy, P. N. Devreotes,** G protein signaling events are activated at the leading edge of chemotactic cells. *Cell*. **95**, 81-91 (1998).
16. **M. Postma, J. Roelofs, J. Goedhart, H. M. Loovers, A. J. Visser, P. J. Van Haastert,** Sensitization of Dictyostelium chemotaxis by phosphoinositide-3-kinase-mediated self-organizing signalling patches. *J Cell Sci.* **117**, 2925-35 (2004).
17. **T. Shibata, M. Nishikawa, S. Matsuoka, M. Ueda**, Modeling the self-organized phosphatidylinositol lipids signaling system in chemotactic cells based on quantitative image analysis. *J. Cell Sci.* **125**, 5138-5150 (2012).
18. **C. A. Parent, P. N. Devreotes**, A cell's sense of direction. *Science*. 284, 765-70 (1999).
19. **T. Shibata, M. Nishikawa, S. Matsuoka, M. Ueda**, Intracellular encoding of spatiotemporal guidance cues in a self-organizing signaling system for chemotaxis in *Dictyostelium cells. Biophys J*. **105**, 2199-209 (2013).
20. **M. Nishikawa, M. Horning, M. Ueda, T. Shibata, Excitable signal transduction** induces both spontaneous and directional cell asymmetries in the phosphatidylinositol lipid signaling system for eukaryotic chemotaxis. *Biophys. J.* **106**, 723-734 (2014).
21. **A. L. Hodgkin, A. F. Huxley**, A quantitative description of membrane current and its application to conduction and excitation in nerve. *J. Physiol.* **117**, 500-544 (1952).
22. **B. Lindner, J. Garcia-Ojalvo, A. Neiman, L. Schimansky-Geier,** Effects of noise in excitable systems. *Physics Reports*. **392**, 321-424 (2004).
23. **S. Fukushima, S. Matsuoka, M. Ueda,** Excitable dynamics of Ras triggers spontaneous symmetry breaking of PIP3 signaling in motile cells. *J. Cell Sci.* **132**, jcs.224121 (2019).
24. **A. Eldar, M. B. Elowitz**, Functional roles for noise in genetic circuits. *Nature.* **467**, 167-173 (2010).
25. **S. Kadar, J. Wang, K. Showalter,** Noise-supported travelling waves in sub-excitable media. *Nature.* **391**, 770-772 (1998).
26. **Y. Zhou, H. Liang, T. Rodkey, N. Ariotti, R. G. Parton, J. F. Hancock,** Signal

integration by lipid-mediated spatial cross talk between Ras nanoclusters. *Mol Cell Biol*. **34**, 862-76 (2014).

27. **Y. Zhou, P. Prakash, H. Liang, K. J. Cho, A. A. Gorfe, J. F. Hancock,** Lipid-Sorting Specificity Encoded in K-Ras Membrane Anchor Regulates Signal Output. *Cell*. **168**, 239-251 (2017).
28. **K. J. Cho, D. van der Hoeven, Y. Zhou, M. Maekawa, X. Ma, W. Chen, G. D. Fairn, J. F. Hancock**, Inhibition of Acid Sphingomyelinase Depletes Cellular Phosphatidylserine and Mislocalizes K-Ras from the Plasma Membrane. *Mol Cell Biol*. **36**, 363-74 (2016).
29. **D. van der Hoeven, K.-J. Cho, Y. Zhou, X. Ma, W. Chen**, **A. Naji, D. Montufar-Solis, Y. Zuo, S. E. Kovar, K. R. Levental, J. A. Frost, R. van der Hoeven, J. F. Hancock**, Sphingomyelin Metabolism Is a Regulator of K-Ras Function. *Mol Cell Biol.* **38**, e00373-17 (2018).
30. **M. Maceyka, S. Spiegel**, Sphingolipid metabolites in inflammatory disease. *Nature*. **510**, 58-67 (2014).
31. **D. van der Hoeven, K. J. Cho, X. Ma, S. Chigurupati, R. G. Parton, J. F. Hancock**, Fendiline inhibits K-Ras plasma membrane localization and blocks K-Ras signal transmission. *Mol Cell Biol.* **33**, 237-51 (2013).
32. **I. A. Prior, C. Muncke, R. G. Parton, J. F. Hancock,** Direct visualization of Ras proteins in spatially distinct cell surface microdomains. *J. Cell Biol.* **160**, 165-170 (2003).
33. **H. Murakoshi, R. Iino, T. Kobayashi, T. Fujiwara, C. Ohshima, A. Yoshimura, A. Kusumi**, Single-molecule imaging analysis of Ras activation in living cells. *Proc Natl Acad Sci USA*. **101**, 7317-22 (2004).
34. **J. F. Hancock, R. G. Parton**, Ras plasma membrane signalling platforms. *Biochem J.* **389**, 1-11 (2005).
35. **S. J. Plowman, C. Muncke, R. G. Parton, J. F. Hancock**, H-ras, K-ras, and inner plasma membrane raft proteins operate in nanoclusters with differential dependence on the actin cytoskeleton. *Proc Natl Acad Sci USA*.**102**, 15500-5 (2005).
36. **J. Y. Tinevez, N. Perry, J. Schindelin, G. M. Hoopes, G. D. Reynolds, E. Laplantine, K. W. Eliceiri,** TrackMate: An open and extensible platform for single-particle tracking. *Methods*, **115**, 80–90 (2017).
37. **S. Matsuoka, M. Ueda**, Mutual inhibition between PTEN and PIP3 generates bistability for polarity in motile cells. *Nature commun.* **9**, 4481-4481 (2018)
38. **S. Funamoto, R. Meili, S. Lee, L. Parry, R. A. Firtel**, Spatial and temporal

regulation of 3-phosphoinositides by PI 3-kinase and PTEN mediates chemotaxis. *Cell.* **109**, 611-623 (2002).

39. **M. Iijima, P. Devreotes**, Tumor suppressor PTEN mediates sensing of chemoattractant gradients. *Cell.* **109**, 599-610 (2002).
40. **A. T. Sasaki, C. Chun, K. Takeda, R. A. Firtel,** Localized Ras signaling at the leading edge regulates PI3K, cell polarity, and directional cell movement. *J. Cell Biol*, **167(3)**, 505-518 (2004).
41. **Chattwood A., Bolourani P. and Weeks G.** (2014). RasG signaling is important for optimal folate chemotaxis in Dictyostelium., *BMC Cell Biol*, **15**, 13.
42. **A. Yamaji, Y. Sekizawa, K. Emoto, H. Sakuraba, K. Inoue, H. Kobayashi, M. Umeda,** Lysenin, a novel sphingomyelin-specific binding protein. *J Biol. Chem.*, **273(9)** 5300-5306 (1998).
43. **M. Abe, T. Kobayashi,** Dynamics of sphingomyelin- and cholesterol-enriched lipid domains during cytokinesis. *Methods Cell Biol.*, **137**, 15-24 (2017).
44. **J.G. Kay, M. Koivusalo, X. Ma, Wohland, T., and Grinstein, S**. Phosphatidylserine dynamics in cellular membranes. *Mol. Biol. Cell,* **23(11)**: 2198-2212 (2012).
45. **H. Takagi, M. J. Sato, T. Yanagida, M. Ueda,** Functional Analysis of Spontaneous Cell Movement under Different Physiological Conditions. *PLOS ONE.* **3**, e2648 (2008).
46. **A. Marchetti, V. Mercanti, S. Cornillon, L. Alibaud, S. J. Charette, P**. **Cosson,** Formation of multivesicular endosomes in *Dictyostelium. J Cell Sci* **117(25)**, 6053–605 (2004).
47. **K. Ravanel, B. D. Chassey, S. Cornillon, M. Benghezal, L. Zulianello, L. Gebbie, F. Letourneur, P. Cosson,** Membrane sorting in the endocytic and phagocytic pathway of *Dictyostelium discoideum. Eur. J. Cell Biol.* **80**, 754-764 (2001).
48. **K.A.K. Tanaka, K.G.N. Suzuki, Y. M. Shirai, S. T. Shibutani, M. S. H. Miyahara, H. Tsuboi, M. Yahara, A.Yoshimura, S. Mayor, ,T.K. Fujiwara, A. Kusumi,** Membrane molecules mobile even after chemical fixation. *Nat Methods,* **7**, 865–866 (2010).
49. **M. Hagedorn, E. M. Neuhaus, T. Soldati,** Optimized fixation and immunofluorescence staining methods for Dictyostelium cells. *Methods Mol Biol.* **346**, 327-38 (2006).
50. **E. Betzig, G. H. Patterson, R. Sougrat, O. W. Lindwasser, S. Olenych, J. S. Bonifacino, M. W. Davidson, J. Lippincott-Schwartz, H. F. Hess**, Imaging

Intracellular Fluorescent Proteins at Nanometer Resolution. *Science*. **313**, 1642-1645 (2006).

51. **L. R. Taylor.** Aggregation, variance and the mean. *Nature*. **189**, 732-735 (1961).
52. **B. D. Ripley**, Modelling spatial patterns. *J. R. Stat. Soc. Series B Stat. Methodol.* **39**, 172-192 (1977).
53. **B. Hopkins, J. G. Skellam,** A new method for determining the type of distribution of plant individuals. *Annals of Botany.* **18**, 213-227 (1954).
54. **Y. Zhou, P. S. Prakash, H. Liang, A. A. Gorfe, J. F. Hancock,** The KRAS and other prenylated polybasic domain membrane anchors recognize phosphatidylserine acyl chain structure. *Proc Natl Acad Sci USA*. **118**, e2014605118 (2021).
55. **M. Maekawa, M. Lee, K. Wei, N. D. Ridgway, G. D**. Fairn, Staurosporines decrease ORMDL proteins and enhance sphingomyelin synthesis resulting in depletion of plasmalemmal phosphatidylserine. *Sci Rep.* **6**, 35762 (2016).
56. **A. D. Tepper, P. Ruurs, T. Wiedmer, P. J. Sims, J. Borst, W. J. van Blitterswijk**, Sphingomyelin hydrolysis to ceramide during the execution phase of apoptosis results from phospholipid scrambling and alters cell-surface morphology. *J Cell Biol.* **150**, 155-64 (2000).
57. **M. Bonomini, S. Dottori, L. Amoroso, A. Arduini, V. Sirolli**, Increased platelet phosphatidylserine exposure and caspase activation in chronic uremia. *J Thromb Haemos*t. **2**, 1275-81 (2004).
58. **T. Tian, A. Harding, K. Inder, S. Plowman, R. G. Parton, J. F. Hancock,** Plasma membrane nanoswitches generate high-fidelity Ras signal transduction. *Nat Cell Biol.* **9**, 905-14 (2007).
59. **T. Gurry, O. Kahramanoğullari, R. G. Endres**, Biophysical mechanism for ras-nanocluster formation and signaling in plasma membrane. *PLOS ONE.* **4**, e6148 (2009).

Publication List

1. **D.Y. Shin, H. Takagi, M. Hiroshima, S.i Matsuoka, M. Ueda,**
   Sphingomyelin metabolism underlies Ras excitability for efficient cell migration and chemotaxis.
   Cell Structure and Function, (2023)
   doi:doi.org/10.1247/csf.23045

Acknowledgements

Osaka University
Prof. Masahiro, Ueda
Dr. Matsuoka Satomi
Prof. Kenji, Matsuno
Mr. Takuma, Degawa
Mr. Seiya Fukushima
Mr. Hidenori, Hashimura
Mr. Yuki, Tanabe
Mr. Kazutoshi, Takebayashi
Mr. Tatsuro, Miyagawa
Mr. Shinichi, Yamazaki
Mr. Daisuke, Yoshioka
Ms. Haruka, Hiraoka
Ms. Mariko, Kurahashi
Ms. Hiroko, Hatagami

Jikei University School of Medicine
Prof. Shuji, Tachibanaki

RIKEN BDR
Dr. Michio, Hiroshima
Dr. Yoichiro, Kamimura
Ms. Shizuka, Taguchi
Ms. Kaori, Tanabe
Ms. Sumire, Hino

Nara Medical University
Dr. Hiroaki, Takagi